Investigation of a Slightly Cooled Integrating Detector (SCID) for Low Level Radiometric Measurements.

Bruce Erwin Adams

A thesis submitted to the faculty of the
Oregon Graduate Institute of Science and Technology
in partial fulfillment of the
requirements for the degree
Masters of Science
in
Applied Physics

August, 1998

The dissertation "Investigation of a cooled detector-integrating amplifier for low level radiometric measurements" by Bruce Adams has been examined and approved by the following Examination Committee:

Raj Solanki, Thesis Adviser
Professor

Anthony E. Bell
Associate Professor

Charles Schietinger
Luxtron Corporation

The Author would like to acknowledge:

Dr. Ray Dils, Dr. Kenneth Wickersheim, Dr. Raj Solanki for their mentorship,

All of the folks at Accufiber Inc. and Luxtron Corporation for their support, particully Charles Schietinger, Earl Jensen, Walt Catino, Bill Pfeifer, and Jon Kirwin who all contributed to this work. Thanks to Stan Grenz for scanning in the graphs, and Mellony Bernal for all those wordprocessing questions.

And especially my wife and daughter, Connie and Alicia, for all of their many sacrifices.

To

My Parents

TABLE OF CONTENTS

List of Tables

List of Figures

ABSTRACT

The goal of this project is to gain a theoretical understanding of the fundamental noise sources in quantum photodetectors and their associated electronics, and investigate practical alternative designs to the traditional transimpedance amplifier (TIA). The limits of electronic noise in TIAs was modeled mathematically, and verified experimentally. This model was used in the design, construction, and evaluation of a switched integrating amplifier. Predictions of the model implied that cooling both the amplifier and the photodetector to 2°C would result in major improvements in performance. Electrical noise measurements were taken on an experimental circuit, and data is presented which agrees well with the theoretical model.

When measuring low photodiode currents (picoamps, at one Hertz bandwidth) with transimpedance designs two major obstacles must be overcome. First, the Johnson noise that is generated in the feedback resistor and second the input offset voltage of the operational amplifier. The offset voltage is very dependent on amplifier temperature and therefore drifts with time. Chopping of the optical input signal or occasionally directly measuring the offset has been the customary solution to this problem. As Johnson noise is a fundamental property of current flowing through a resistor, it sets the limit for the minimum detectable photodiode current. Johnson noise is proportional to absolute temperature of the resistor, therefore to reduce the noise an order of magnitude requires cooling from 300°K to 30°K. The technology required to accomplish this level of cooling is impractical or too costly for most industrial applications.

If a capacitor is substituted for the feedback resistor the transimpedance amplifier is transformed into an integrator. A perfect capacitor has no resistive component, and therefore produces no Johnson noise. Dynamic range and bandwidth are determined by varying the integration time. The next two limiting noise sources are from the photodiode. These twos sources sum together and reduce mathematically to be equivalent in form to

Johnson noise. This sum (kT/R) is inversely proportional to the dynamic impedance of the diode which is very temperature dependent. A 25°C decrease in diode temperature below ambient can increase the dynamic impedance by an order of magnitude, thus modest cooling dramatically lowers the photodiode component of noise.

Operational amplifier input offset voltage is also a strong function of temperature. The same 25°C decrease in temperature will also reduce the offset voltage by more than an order of magnitude, and greatly reduce sensitivity to changes in temperature. Thus a photodiode and an integrator operating at 25°C to 50°C below ambient, could side step the major limitations of transimpedance amplifiers, i.e. offset errors, Johnson noise from the feedback resistor, and the photodiode contribution to noise.

Thus a Slightly Cooled Integrating Detector (SCID) would find applications in many areas which require the sensitivity of photomultiplier tubes, and the robustness of solid state designs. Examples are found in semiconductor wafer processing, aluminum sheet manufacturing, and fiberoptic immunosensors.

CHAPTER 1

INTRODUCTION

1.1 Overview - Photovoltaic (PV) Detectors for Medical, Scientific, and Industrial Instrumentation

The commercial availability of high numeric aperture multimode optical fibers has made practical many new types of optical fiber sensors [1-4]. These new technologies are germinating the development of simple robust instruments for real-time measurement in harsh industrial environments.. The dynamic range and sensitivity of the systems are often limited by the optical detector technology and many important industrial applications can not be implemented with the size, weight, fragility, and cost associated with photomultiplier tubes. Thus the use of inexpensive low noise detection paradigms will extend these sensor technologies into new markets if methods can be found to decrease the noise limits imposed by the traditional transimpedance amplifier [5].

1.1.1 Opportunities for chemical sensor applications addressed by improved detector technology.

Contamination of the environment is recognized as one of the major worldwide problems. New technologies must be developed to monitor the many complex changes introduced by human activity in the biosphere. These measurements are typically performed by collecting field samples of the contaminated material, extraction of the organic chemicals (if necessary) and laboratory analysis, usually by gas chromatography or high performance liquid chromatography. The collection and handling of samples involves significant time and expense. In order to streamline the process of trace organic analysis, better on-site detection and measurement techniques are needed.

The techniques investigated in this thesis could make practical industrial instruments for the measurement of trace organic chemicals, pesticide and herbicide residues in soils, groundwater, drinking water, industrial waste, tank leak detection, remote monitoring, clean-up site analysis, etc. Commercial versions of this sensor/detector technology can be used to monitor; public water supplies for microbes, public places for airborne diseases, pollution monitoring, biomedical applications (including blood gas analysis), food testing (especially determining the presence of Botulism, Salmonella, and E. Coli), pharmaceutical research and process control, explosives and drug detection, and the detection and monitoring of other toxic materials. There is a significant commercial interest in the development of on-site monitors for benzene, as an indicator of gasoline storage leakage.

There are a wide variety of needs for improved monitoring and analysis of trace chemicals in several different industries. These needs are increasingly being addressed with immunoassays specific for individual analytes or for restricted chemical classes. Immunoassays have provided one of the best approaches for on-site analysis. The highly selective binding of the antibody provides a molecular recognition based on the actual shape and charge distribution of the analyte. Currently, new immunoassays for chemically hazardous materials such as pesticides, herbicides, polychlorinated biphenyls, and petroleum

hydrocarbons have become available [6-8].

Presently, a variety of immunoassays are being offered as kits, similar to the pregnancy test kits, which are a one shot, low cost disposable measurement. These assay kits offer a significant improvement over traditional methods for trace analysis of organic compounds. The ability to get quantitative analysis results without sending samples to a remote laboratory can improve many phases of an environmental characterization and cleanup effort. In addition to the cost saved on sample packaging, transportation and laboratory analysis, the shortened response time for analysis can greatly improve the overall efficiency of the operation. The major draw-back to the kits is the irreversible nature of the measurement. There is an obvious need for a real time or near real time reversible in-situ measurement for continuous monitoring and process control.

Fiber-optic immunoassays based on Evanescent-Wave Spectroscopy (EWS) has proven capable of especially low detection thresholds. Thresholds as low as 30 picomoles have been obtained for botulinum toxin [2] and detection limits in the femto-molar range have been achieved [6]. Most implementations of this approach have been for large biological molecules such as proteins, although there has been some work on fiber-optic assays for small molecules. A recent implementation of a fiber-optic immunoassay for the herbicide Atrazine has been reported [3,7,8]. Evanescent-wave fiber-optic immunoassays for drugs and explosives are also known to be under development.

The current generation of EWS use lasers to stimulate fluorescent labels at the tip of fiberoptic probes, where the fluorescent signal is coupled back to a chopper / photomultiplier tube for detection. Even though these systems are highly sensitive, they are fragile, bulky, costly, and require high voltage power supplies. As the requirements for chemical sensor application are low in signal bandwidth (a few measurements per minute), a charge integrating quantum detector optimized for low noise detection could potentially obtain the required sensitivity for these measurements. Thus it seems as though a large market exists for a detector which would enable these immunosensor technologies to be implemented into a practical design.

1.1.2 Opportunities for low noise Optical Fiber Thermometry (OFT) in the Semiconductor Industry.

As semiconductor processes evolve to keep pace with market demands, geometries are becoming smaller, junctions shallower, and films thinner to achieve higher speeds and device densities. This greatly increases the requirement for precise temperature measurement and control. As a direct consequence of shallower junctions, the thermal budgets are smaller thus process temperatures are progressively being forced lower.

Over the last decade Optical Fiber Thermometry (OFT) has become accepted as a solution to temperature measurement in several key semiconductor processes [4,9]. In-situ emissivity and temperature measurements using the "Ripple Technique" has been implemented into Rapid Thermal Processing (RTP) [10-13]. Chemical Vapor Deposition (CVD) has used the qualities of low drift, high resolution, and ease of wafer back-side surface measurements to improve process quality. Tungsten silicide deposition at 550°C has been successfully implemented with optical fiber thermometers.

Many attempts have been made to use infrared pyrometry with wavelength sensitivities in the 4 to 10 micrometer region, which corresponds to the region of peak spectral emission from objects in these lower temperature processes. These attempts have been largely unsuccessful for both fundamental and practical reasons which are detailed as follows:

1) The bandgap of single crystal silicon at room temperature is too large to absorb radiant energy longer then about one micrometer in wavelength [9]. As the temperature increases up to around 700°C the absorbance of energy of wavelength longer than one micrometer increases due to thermal generation of electron-hole pairs which causes the free-carrier concentration to increase. This increase in free-carrier concentration results in an increased absorption which is important even in lightly doped wafers. Because of temperature dependance of the band structure, the

absorption edge shifts to longer wavelengths with an increase in temperature. The shape of the band edge changes with temperature in phonon dependent indirect band-gap materials like silicon. The increase in phonon population with temperature also increases and modifies the lattice absorption peaks as well [9,14]. Therefore, the emissivity and absorptivity are low in silicon at room temperature for radiation of wavelengths greater than one micrometer. As the silicon temperature increases up to 600°C the emissivity and absorptivity dramatically increase to higher values. For wavelengths shorter than one micrometer, the wafers are opaque, emissivities high, and the optical properties are not strongly dependent on temperature.

2) In designing a thermometer it is desirable to obtain a large change in signal for a small change in temperature, i.e. a high sensitivity. If we thus define Pyrometric Sensitivity S as a fractional change in radiant energy I, for a fractional change in absolute temperature T.

$$S \equiv \frac{\frac{\Delta I}{I}}{\frac{\Delta T}{T}} = \frac{T}{I}\frac{\Delta I}{\Delta T} \qquad (1.0)$$

We can determine the spectral radiance by Planck's equation;

$$I = \frac{C_1}{\lambda^5 \left\{ e^{\frac{C_2}{\lambda T}} - 1 \right\}} \qquad (1.1)$$

where $c_1 = 1.191044 \times 10^8\ W\mu m^4 m^{-2} sr^{-1}$, $c_2 = 14388$ micrometers Kelvin, lambda is

the wavelength in micrometers (in vacuum), and T is the absolute temperature in degrees Kelvin.

By differentiating Planck's equation with respect to temperature and substituting back into the sensitivity equation (Eq 1.0) we obtain;

$$S = \frac{C_2}{\lambda T} \frac{e^{\frac{C_2}{\lambda T}}}{e^{\frac{C_2}{\lambda T}} - 1} \qquad (1.2)$$

for wavelengths around one micrometer and temperatures around 800°K, $\exp(C_2/\lambda T)$ is nearly 65 million, therefore Eq 1.2 simplifies to;

$$S \approx \frac{C_2}{\lambda T} \qquad (1.3)$$

This simple relationship shows that a pyrometer with a one micrometer wavelength detector is five times more sensitive to a change in signal than a five micrometer detector, even though the radiant intensity at 350°C is over four million times greater for the longer wavelength! For example, consider the temperature measurement of a surface where the uncertainty in emissivity creates an error of 1°C when measured with a pyrometer sensitive to one micrometer wavelength. This same uncertainty in radiance measurement will create a 5°C error when the measurement is made at 5 micrometer wavelength as can be seen in equating equations 1.0 and 1.3.

IR detectors with greater than 2μm wavelengths have additional features which have made them impractical outside the laboratory environment. Because of the low photon energy of the infrared wavelengths, thermal noise will dominate over the signal unless the

detectors are cooled, often to cryogenic levels. This level of cooling involves sealing the detectors in dewars for insulation and cooling. The use of liquid nitrogen or other IR detectors of this category are often slow in response, variable in sensitivity, and require chopping of the optical signal with a lock-in amplifier. These systems are, bulky, fragile, very expensive and require continual maintenance and therefore are not candidate for industrial instrumentation which must function for years in harsh environments without attention.

There is a very large industrial opportunity for measuring temperature below 350°C for many current semiconductor processes. The use of standard infrared technologies for these applications fall short for the reasons mentioned above, and the use of near infrared (NIR) quantum detectors are not presently used because of the extremely low levels of radiant flux at the shorter wavelengths. The current output from a practical industrial fiber optic thermometer with a silicon photodiode measuring a 200°C target would be 10^{-16} amps. The goal of this thesis is to explore the theoretical and practical limitations of designing industrial NIR detector for measuring tiny currents of this magnitude.

1.1.3 Opportunities for low noise Optical Fiber Thermometry in the Aluminum Industry.

The use of aluminum for beverage containers has become very popular as it offers many advantages over the heavier and more fragile glass bottles. Aluminum has the additional advantages of ease of handling and separating in the waste stream, with simple and low energy recycling steps. The increased demand for aluminum sheet feed stock has focused attention on the rolling technology by which it is formed.

Aluminum billets are rolled back and forth through rollers until it is transformed into the thin sheets used by the beverage industry. The temperature at which the rolling process occurs is very crucial in determining the final quality of the product. The rolling process

itself adds heat to the system, and the speed and pressure of the rollers are varied to help maintain correct rolling temperature.

One historical problem which has limited the control of quality in the rolling process is real time knowledge of the aluminum sheet temperature. Contact probes like thermocouples and RTDs are not practical because of their inability to establish thermal contact on a rapidly shifting and gyrating object. The surface of the sheet is coated with an organic (fish oil) to aid in the rolling process. This limits the effectiveness of heat transfer to quasi-contact methods.

Non contact radiation pyrometry would seem like the obvious solution to this problem, but its practical implementation has failed to correctly address the important and difficult emissivity issues. The emissivity of clean sheet aluminum is very low, around 0.01 or less, and varies as it is processed due primarily from the texture imparted to the surface from the stretching and rolling. The lubricants added to the surface (non uniformly) drastically modify the emissivity in the infrared portion of the spectrum. Traditional infrared pyrometers sensitive in the 200°C to 400°C range are greatly affected by these changes .

Integrating a more sensitive detector into a Ripple Pyrometer [10-13], would allow for detection of radiation at wavelengths less affected by uncertainty in emissivity, and could track the emissivity changes in real time and *in-situ*. This application is not unlike many which are becoming important in Physical Vapor Deposition (PVD) and Chemical Vapor Deposition (CVD) in the semiconductor industry.

1.2 Transimpedance Amplifiers (TIA) with Photovoltaic Detectors; Their strengths and limits.

Photocells are produced by forming a diode junction of P and N type semiconductor material. Upon physical contact, electrons flow from the N to P type material. The electron flow (and complementary flow of holes in the opposite direction) forms a thin volume at the

junction devoid of current carriers called a depletion zone. The electrons/holes continue to flow across the junction until the resulting voltage gradient produced across the depletion zone is equal to the contact potential difference of the two materials. When radiant energy greater than the band gap of the semiconductor material (1.12 ev for Silicon, and 1.8 ev for GaAsP) pass through the photodiode, some of the valence electrons are transported into the conduction band by adsorption of photons. This process leaves behind positive holes in the valence band, so that the photon energy has gone into the creation of electron/hole pairs. Electron/hole pairs are generated in the depletion layer as well as in the N and P doped materials. Electrons generated in the depletion layer drift to the N doped material and holes will drift to the P doped material. Also, electrons generated within the P layer and holes generated within the N layer will drift to the depletion zone, if they are within the diffusion length. The net result is that charge accumulates in the N and P layers proportional to the electron/hole pair creation from photon absorption (photovoltaic effect). In practical photodiode devices, the P layer is made as thin and transparent as possible, the depletion layer as thick as possible, to maximize the chance of photon absorption, thus yielding higher quantum efficiencies.

If the photocell terminals are left unconnected while the device is exposed to radiation it will continue to accumulate charge until the shift in the Fermi level due to charge transfer is equal to the potential barrier. This is the open circuit voltage V_{OP}. If the photocell terminals are shorted together the current flow is known as short circuit current I_{SH}.

In the unilluminated state the voltage/current characteristics of photodiodes are very similar to a conventional semiconductor diode (*Figure 1.1*).

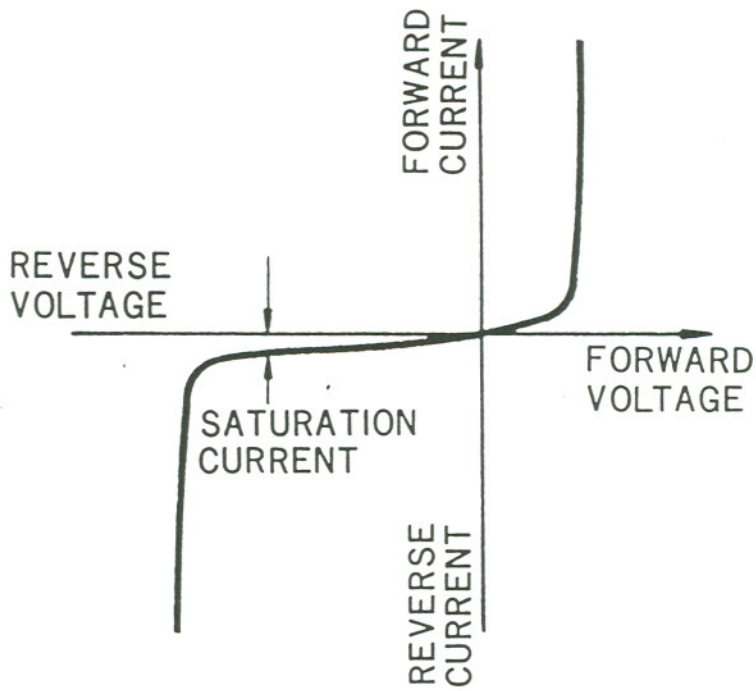

Figure 1.1 V-I curve for unilluminated photodiode

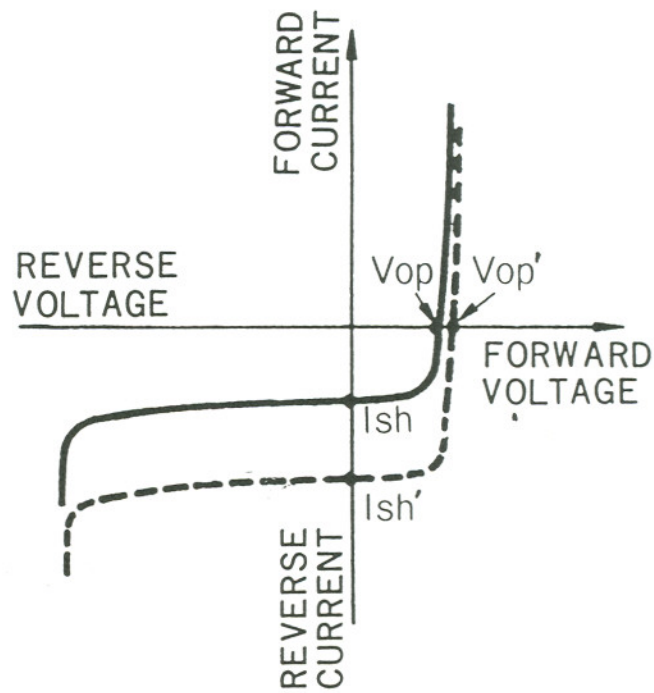

Figure 1.2 V-I curves for different values of irradiance

However, when photons are absorbed and generate electron-hole pairs, the V-I curve is progressively shifted down as the irradiant intensity is increased. For a given irradiance, the open circuit voltage and short circuit current are found at the intersection with the axis of the V-I graph (*Figure 1.2*).

For changes in irradiance onto the diode, I_{SH} is quite linear over 6 to 8 orders of magnitude, where as V_{OP} changes logarithmicly. The use of a transimpedance amplifier (an operational amplifier with negative resistive feedback), which has almost zero input impedance, will allow current to be drawn off from the photodiode while keeping it effectively short circuited. This is the photoconductive mode of operation. Although the frequency response of the circuit is modest, as the carriers are not quickly removed by the effects of an external bias, it is quite adequate for the bulk of industrial radiometric applications which are less than 10khz bandwidth.

For any real operational amplifier the input impedance is not truly zero, which results in a bias current that produces a measurement error. Bipolar Op-Amps have bias currents of several nanoamps to several hundred nanoamps. FET Op-Amps are a better choice for low level detection with bias currents of ten picoamps or less. These currents are highly dependant on ambient temperature. This varying current gets amplified along with the signal and becomes a major source of electronic drift. Traditionally, this problem has been resolved by "Chopping" the signal with a reference, or auto calibration circuits which adjust out the offset at frequent intervals.

An alternative to linear transimpedance amplifiers is the use of logarithmic amplifiers. This is the method traditionally employed in optical pyrometers up to the mid 1980's when microprocessors and digital technology begin to replace analog designs for industrial instruments. This technique would place the photodiode onto a high impedance amplifier (photovoltaic mode) resulting in a logarithmic voltage output V_{OP} as a function of input radiance. This logarithmic response was matched by placing a diode in the feedback loop of the operational amplifier. This analog circuit allowed for a very wide dynamic range, and biasing the diode improved both speed and linearity. This method is

unacceptable for precision low level radiance measurements because the diodes are extremely sensitive to changes in ambient temperature. Additionally, the bias voltage, which appears across the diode produces a dark current. The dark current generates an additional component of Shot noise which limits this design for use in low level detection.

Although the linear amplifiers are well suited for precision measurements, they lack the wide dynamic range necessary for applications such as radiation pyrometry where a change of temperature from 500°C to 1900°C corresponds to six orders of magnitude change in photodetector current. Some form of automatic gain or offset switching is required to obtain the necessary range, which brings with it problems associated with switching time, contact noise, and system stability. Although there are practical solutions to these problems, they carry with them limitations in measurement bandwidth and reliability, with associated increase in complexity and cost.

In summary, the traditional approach for low level radiance measurements in industrial (non-laboratory) instrumentation, is to use a photodiode in the photoconductive mode with a FET input transimpedance amplifier. This system will be modeled to determined the fundamental limits of detectability.

1.3 A New Paradigm - A Slightly Cooled Integrating Detector (SCID) with a Lower Noise Floor

The thesis presented here is to identify and remove the limiting noise sources for the standard combination of a transimpedance amplifier driven by a photodiode in the photovoltaic mode. By replacing the feedback resistor with a capacitor, the major Johnson noise source is eliminated. The second largest term is Shot noise due to thermally induced currents in the photodetector. This term is inversely proportional to the dynamic impedance, and the dynamic impedance is very sensitive to temperature and may increase by an order of magnitude if the temperature is reduced by 25°C. Thus, this noise term can be greatly reduced by modest cooling of the photodetector. The third category of noise is the voltage

offset which is sensitive to ambient temperature, but becomes small and insensitive to ambient drifts below 0°C. The forth and fifth noise sources are the voltage and current noise from the input of the operational amplifier. These terms are exponentially related to temperature like the dynamic impedance, and will be largely attenuated by a simple decrease in amplifier temperature.

1.4 General Summary

The above analysis suggests that by modestly cooling a photodetector and a integrating amplifier both to zero Centigrade many noise sources which limit the traditional transimpedance designs will be eliminated or greatly reduced. Johnson noise in the feedback circuit will have been eliminated, and Johnson and Shot noise in the photodiode will be significantly reduced. This slightly cooled combination could be manufactured with low cost solid state technologies which would provide the robustness required for most industrial applications. There are many industrial markets such as; semiconductor processing, metals processing, and biochemical analysis, which could use this technology.

In chapter two the various noise sources will be described, and a mathematical model will be developed to predict the total noise characteristics of a photovoltaic photodetector/JFET transimpedance amplifier combination. This model will be developed to predict the effects of changes in ambient temperature. This model will be confirmed by experimental measurements. In chapter three, the total noise model will be modified for the integrating amplifier, and predictions will be made as to the noise characteristics as the ambient temperature drops to two degrees centigrade. The integrating amplifiers, with switches and capacitors offer additional noise sources that must be modeled and measured to confirm that a true noise reduction can be realized. Experimental data from a slightly cooled integrating detector (SCID) will be presented. Chapter four will compare the noise and dynamic range between the transimpedance and switched integrator technologies. Conclusions from the presented work will be discussed and the implications which it may

have upon instrument design and performance will be elucidated. The potential of a hybrid design will be considered.

CHAPTER 2

THE TRADITIONAL APPROACH TO LOW NOISE DETECTION

2.1 A Mathematical Model for Predicting the Noise Limitations in the Traditional PV Detector / JFET Transimpedance Amplifier Combination.

In this section various noise terms will be described and mathematically quantified. The total noise will be predicted by taking the square root of the sum of the squares of all these uncorrelated noise sources. These noise terms will be developed as a function of ambient temperature in order to understand the effects of cooling. The system to be analyzed is the Hamamatsu 1337 photodetector operated in the photovoltaic mode in conjunction with the OPA111 (Burr-Brown) operational amplifier configured as a transimpedance amplifier. See *figure 2.1* for a schematic diagram of the transimpedance noise model. This model will be developed in a general format on a spreadsheet so it may be easily modified for predicting performance of a switched integrating amplifier. The temperature dependance of feedback resistors, photodiodes, and amplifiers will be determined independently to allow these effects to be evaluated separately.

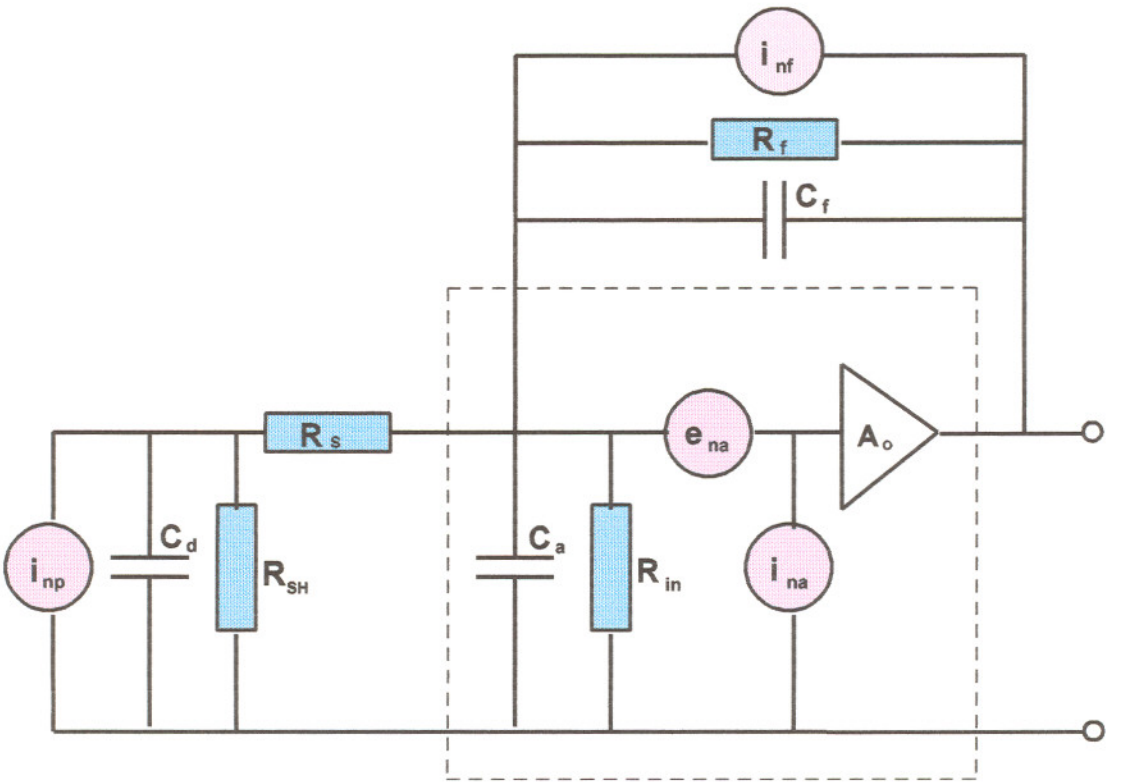

Figure 2.1 Schematic diagram of the noise model for a transimpedance amplifier with a photodiode in photovoltaic mode.

2.2 Intrinsic and Extrinsic Noise

Significant noise sources in the electro-optics have been studied and categorized since Schottky's work in 1918 [15]. A complete quantitative description of all aspects of these sources still awaits elucidation, but renewed interest has recently developed with the development of new mathematical techniques. This description will focus around noise intrinsic to the system [16-20], that is to say, fundamentally inherent to the Physics of the optics or electronics, as opposed to noise sources extrinsic to the system, such as those induced by electromagnetic radiation or capacitive coupling. These extrinsic noise sources are addressed by various circuit layout and design techniques, proper shielding and

grounding methods, power supply and digital noise isolation, and component selection [21-24]. In the majority of commercial circuits it is these practical extrinsic designs issues that determine the limiting noise characteristics of the system. In this analysis it is considered that the extrinsic noise has been reduced to the level that intrinsic noise becomes the limiting factor.

2.3 Optical Throughput versus Electrical Gain.

Although it may seem obvious, the importance of collecting as much optical signal by the optical system prior to conversion to an electrical signal is hard to overemphasize. Increasing optical signal gain can be accomplished before the fundamental electrical noise is added to the signal, and therefore will increase the signal to noise ratio. Increasing the signal will increase the signal Shot noise by the square root of the signal magnitude, so the signal to noise improves. Once the intrinsic white electrical noise (of the same bandwidth) is added to the signal, the two become indistinguishable, and an upper limit of signal to noise is fixed. Maximizing optical throughput involves the system clear aperture, the numeric aperture (a measure of the field of view of the sensor), and the optical bandwidth (the range of wavelengths to which the system responds). These factors clearly are application specific, and must be balanced against the need for a small area detector to minimize electrical noise. As an example, if the application is to measure the temperature of a silicon wafer, one is constrained by the wafer becoming partly transparent to wavelengths longer than one micrometer. Physical access to the wafer may limit the field of view, and thermal perturbations of the wafer temperature uniformity may limit the clear aperture.

The method of detecting also influences the signal before electrical noise is mixed in. In general, for a TIA, the signal increases proportionally to the feedback resistor, and the Johnson noise from the feedback resistor increases with the square root of the resistance. Therefore, the highest practical value of feedback resistor is often chosen. This value is

limited when the parasitic capacitance and leakage become overriding factors (commonly above 100M ohms).

By forward biasing the photodiode (photoconductive mode) the resulting photoconductive gain could be as large as several thousand, depending on the detector type and the electric field. This is commonly done in communications circuitry as it greatly increases the responsiveness of the detector, allowing greater transmission bandwidths. For low bandwidth (very low noise applications), the bias voltage creates a large dark current through the detector. The Shot noise from this current becomes a limiting factor. Avalanche Photodiodes (APD) and Photomultiplier Tubes (PMT) may have gains of 10^5 or 10^6 and can be used as discrete photon counters. The increased signal to noise must be balanced against the complexity of the associated circuitry, limited dynamic range, fragility, bulk, and cost.

2.4 Intrinsic Noise Sources, Offset Errors, and their Temperature Dependance.

The following potentially significant sources of noise will be quantified mathematically for developing a noise model as a function of ambient temperature and photodiode current. They are Shot noise, Johnson noise, Flicker or 1/f noise, voltage and current noise from the amplifier, amplifier offset voltage and current errors, drift errors, and kT/C errors.

2.4.1 Shot Noise

Shot noise is produced by the random fluctuation of carriers diffusing across a potential barrier [15, 20-22]. A physical analogy to electrical Shot noise might be the sound of rain on a roof top. Each drop has about the same energy (e), the current would be related to the number of drops per second (I), and the area of the roof is proportional to bandwidth

(Δf). While rain is falling it produces no noise, only when it reaches the barrier of the roof are the variation in flow detected.

In junction devices, random thermal motion causes variations in diffusion rates in the neutral zone and variations in the generation-recombination rates in both the neutral and depletion regions. To derive an expression for Shot Noise in a diode (photodiode) we assume the arrival rate (dN/dt) of carriers reaching the diode junction is random (Gaussian), and therefore the following statistical relationship for the variation (δ dN/dt) holds.

$$\delta \, dN/dt = [2 \, (dN/dt) \, \Delta f]^{1/2} \tag{2.1}$$

By definition, current is the rate of change of charge or the rate of carriers times the charge per carrier.

$$I = dq/dt = d(Ne)/dt = e \, dN/dt \tag{2.2}$$

Therefore, combining equations 2.1 and 2.2, we can derive a relationship for noise current i_n^2 due to Shot Noise.

$$i_n^2 = 2Ie\Delta f \tag{2.3}$$

which is truly independent of the source that generates the carriers. The component of Shot Noise produced from the carriers generated photons (equation 2.5) can be calculated by substituting the photon generated current (equation 2.4) into the expression for Shot Noise current (equation 2.3).

$$I = \eta Q A_d e \tag{2.4}$$

where A_d = detector area, η = quantum efficiency, Q = radiant photon incidence, e = electric

charge.

$$i_n^2 = 2\eta Q A_d e \Delta f \qquad (2.5)$$

The Shot Noise component produced from carriers induced thermally is calculated from the diode current-voltage characteristics given by;

$$I = I_s (e^{(eV/kT)} - 1) \qquad (2.6)$$

where e = electric charge = 1.6×10^{-19} (Coulombs), V= Potential Difference in Volts, k=Boltzmann's constant= 1.38×10^{-23} (J/K), T= Absolute Temperature (Kelvin), I_s= Reverse Saturation Current (Amps). This equation is really the sum of two currents flowing in opposite directions, the thermally generated minority carriers, and the diffusion of majority carriers across the junction. The two currents are independent and uncorrelated so the noise equation must be applied to each separately. Even thought the currents flow in opposite directions, the noise generated by them adds together. The root sum of the squares results in;

$$i_n^2 = 2 I_s (e^{(eV/kT)} + 1) e \Delta f \qquad (2.7)$$

We can determine the dynamic impedance by differentiating the Schottky relation (equation 2.6) with respect to voltage.

$$1/R_0 = dI/dV = (I_s e/kT) e^{(eV/kT)} \qquad (2.8)$$

Substituting $I_s e$ back into equation 2.7 to eliminate I_s yields;

$$i_n^2 = 2\,(kT/R_0)\,(e^{-eV/kT})\,(e^{eV/kT} + 1)\,\Delta f \qquad (2.9)$$

If the photodiode has zero bias voltage across it, as in the ideal photovoltaic mode, equation 2.9 reduces to a simplified expression for the thermally generated Shot Noise.

$$i_n^2 = 4kT\Delta f / R_0 \qquad (2.10)$$

The term R_0 has been derived from the slope of the I/V curve at zero bias voltage across an ideal diode. Real diodes have leakage that acts in parallel with the thermally generated Shot Noise.

The amount of noise that is measured will depend on the bandwidth of the measurement. The longer you look, the more noise you will see! 1/f (pink) noise and much of induced noise have spectral dependencies which must be considered. It is therefore convenient to express noise terms as the square divided by bandwidth. Noise terms add by the Root of the Sum of the Squares (RSS), so the Noise Spectral Density terms will add linearly.

Adding the Noise Spectral Densities from the photodiode resistance (leakage) Johnson Noise (Eq 2.9) to the thermally generated Shot Noise (Eq 2.10) yields,

$$i_n^2/\Delta f = 4kT/R_0(\text{thermal}) + 4kT/R_{leakage} = 4kT/R_m(\text{measured}) \qquad (2.11)$$

where R_m is the actual measured value of resistance. Keep in mind that R_0, the thermally generated component, is a very strong function of temperature. The majority of the diode temperature dependance is accounted for by changes in the saturation current as described by the following function [51];

$$I_s(\text{at } T_n) = I_s(\text{at } T_r)\, T_n^{(S/N)}\, e^{\{-qE_g(1-T_n)\,/\,(NkT_n)\}} \qquad (2.12)$$

where I_s is diode saturation current, T_r is the diode reference temperature given in specifications, T_n is the new operating temperature, S is the saturation current temperature exponent (default = 3.0), N is the emission coefficient (default = 1.0), and E_g is the energy gap (default = 1.11ev).

One additional note on the properties of Shot noise. Shot noise only exists when a charge crosses a potential barrier as in a PN junction or cathode to anode of a vacuum tube where there are uninterrupted transits between electrodes. There exists the effect of the space-charge which smooths the current and undermines the assumptions of purely random electron flow. For this reason there is little or no Shot noise generated in a conductor, and the application of Shot noise theory is limited in solid state devices.

2.4.2 Johnson Noise

Johnson Noise (also known as Thermal, Temperature, or Nyquist Noise) is a fundamental property of any resistive element. It was first observed by J. B. Johnson in 1927 who found that it was related to absolute temperature. In 1928 Nyquist at Bell Labs developed a theoretical description based on Brownian movement within an electron gas [25]. He was able to quantify that the noise current spectral density is;

$$i_j^2/\Delta f = 4kT/R \qquad (2.13)$$

The statistical variations in electron concentration create fluctuations in voltage or current which are independent of current flow. Even an unconnected resistor sitting on the table will show this tiny noise across the leads. It is interesting that this intrinsic noise source depends only on temperature and resistance and is totally independent on the composition of the electrical components. Johnson noise demonstrates a uniform power distribution over all frequencies and is therefore considered "white" like Shot noise.

The Norton equivalent circuit for a "real" resistor is a "noiseless" idealized resistor in parallel with a Johnson noise current source as shown below [23]. Current noise source are used on the amplifier input as input currents are amplified into output voltages in a transimpedance designs. To express the Johnson noise as a voltage one would use the Thevenin equivalent circuit. The Thevenin circuit would consist of an idealized noiseless resistor in series with a Johnson voltage noise source.

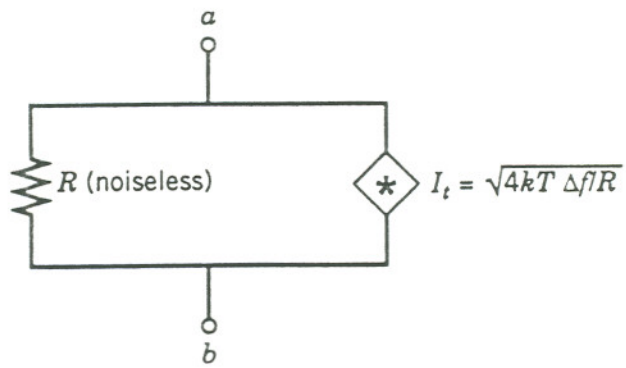

Fig. 2.2 Johnson noise in a resistor is represented by an equilivent circuit of "noiseless" resistor in parallel with Johnson noise current source.

2.4.3 kT/C Noise

The Johnson noise expression in terms of voltage $V_J = (4ktR\Delta f)^{1/2}$ implies that an infinite resistance (an open circuit) would generate infinite noise [23]. This is not seen because all real circuits have some amount of shunting capacitance (C) across the resistance which limits the voltage. There is an interesting trade-off that works as follows. If the resistance goes up, so does the Johnson noise by the square root of R as predicted from the above equation. But as the resistance goes up the bandwidth goes down as the cut-off

frequency is determined from the RC time constant. So as the resistance increases, the noise spectrum yields higher noise at lower frequencies. If one integrates the noise spectral density over frequency the total noise in mean squared volts is kT/C, independent of the value of resistance. This noise limit becomes important in sample and hold circuits, A/D converters, and switched capacitor circuits, which operate at high bandwidths with very low capacitance.

The TIA used in this study for a reference has 330pF in parallel with the feedback resistor, and looks at a photodiode with 380pF capacitance. The switched integrator looks at 65pF photodiode capacitance with 100pF as the smallest value of integrating capacitance. The kT/C noise voltage for 100pF at 300 Kelvin is 41pV. This small value will have no impact on these low bandwidth applications considered in this thesis.

2.4.4 1/f Noise

1/f Noise or "**Low Frequency Noise**" has a very interesting history and is currently a topic of research in many different fields. One might argue that because there is not a "theoretical mechanism" from which a mathematical description can be derived that 1/f noise should be considered an "extrinsic" rather than an "intrinsic" source of noise. It is really more of a syndrome being defined by the symptoms, than a disease, which is defined by a specific underling mechanism. Even so, the ubiquitous nature of 1/f noise makes it difficult to eliminate from a theoretical treatment of noise if one is striving to obtain descriptions of practical devices designed to be stable and operate at low frequencies. Low frequency noise measurements of a few cycles per day still show the 1/f power spectrum, and therefore it is usually the largest component of noise in very low frequency circuits. 1/f Noise has spectral characteristics that approximate constant power per decade of frequency which results in the noise power being inversely related to frequency. Because the noise spectrum is weighted toward the longer wavelengths, it is called "**Pink Noise**", by analogy with light. This is in contrast with Shot and Johnson noise which have constant

power per hertz and are analogous to white light. There are probably many different causes of 1/f noise in electronic circuits and it has received different names under different circumstances.

When the electrical conductivity fluctuates at the junction of two different materials it is called "**Contact Noise**". This is important in relays, switches, lead contacts to semiconductors and integrated circuits, composition resistors, and carbon microphones. The noise caused by leakage around the feedback resistor on very high gain transimpedance amplifiers has a 1/f spectrum. In vacuum tubes it is observed as "**Flicker Noise**", and is sometimes attributed to the cathodes slowly varying efficiency of emitting electrons. In semiconductor devices it is called "**Modulation Noise**" and is associated with crystal imperfections, surface traps, and surface leakage currents.

In real resistors the "**Excess Noise**" above the Johnson Noise limit is due to the fluctuation in resistance, and depends on the materials and methods of resistor construction. Horowitz and Hill [21] list some typical excess noise values given as RMS microvolts per volt applied across the resistor, measured over one decade of frequency:

Carbon-composition	0.10μV to 3.0μV
Carbon-film	0.05μV to 0.3μV
Metal-film	0.02μV to 0.2μV
Wire-wound	0.01μV to 0.2μV

A generalized expression for 1/f noise current is given by Dennis (24)

$$i_{1/f}^2 = k I_B^{\alpha} \Delta f / f^{\beta} \qquad (2.14)$$

where k is a proportionality constant, I_B is the bias current and α is approximately equal to 2 and β is in the range of 0.8 to 1.5.

It is interesting to note that 1/f noise appears in all sorts of phenomena outside the area of electronics, and a quick search of the web will demonstrate it is a current topic, readdressing some of the old problems with the newer mathematical tools like fractals and self-organized structures [26-29]. It can be shown in linear systems that 1/f noise results in random processes expressible as a product of several random variables [30-32].

In biological system 1/f noise has been described in DNA sequences, neural populations, and heartbeats [33-35]. In Astronomy, aperiodic variability in the X-ray emission of Cygnus X-1 [36] and analysis of interplanetary magnetic fields [37]. If one measures the loudness of classical music over time, it follows a 1/f spectrum [38], or the fluctuation of the flow of traffic on an expressway [39-41], or the granular flow of sand (as in a hourglass) [42], chemical corrosion measurements [43], populations densities, ecology and evolution [44,45], radioactive decay [46], light intensity fluctuations in photon counting [47], and in economics and financial markets [48,49], the speed of ocean currents or the yearly flow of the Nile measured over the last 2000 years [21].

Some of the older texts on noise list **Popcorn** noise (**Burst** noise) as a category separate from 1/f. It has a power spectrum of $1/f^2$ which is referred to as "red noise". I believe the current view is to treat these "red" sources as part of a generalized form of $1/f^{\beta}$ noise. Other $1/f^{\beta}$ noise sources with a high β are the fluctuations of the frequency of rotation of the earth where $\beta = 2$, and the power spectral density of galactic radiation noise $\beta = 2.7$.

Popcorn noise appears in burst and causes a discrete and transient shift in the baseline. The burst duration varies from microseconds to seconds, and occur at frequencies of hundreds per seconds to a few per minute. The amplitude is constant and is determined by the nature of the specific defect which causes it. In some cases, Popcorn noise is several hundred times the amplitude of Johnson noise. It was generally seen in high impedance operational amplifiers and is attributed to metallic impurities creating defects in the junction. This type of noise has been eliminated in current IC operational amplifiers by cleaner manufacturing processes. It is important in this study because noise of similar form has been observed in the integrating amplifier and as will be shown later was subsequently

attributed to cosmic and background radiation, or in another instance, leakage from contamination around the feedback resistor.

At first thought it might seem that 1/f noise would produce nearly infinite noise as one approached D.C. measurements. In practice, every instrument has a measurement bandwidth determined by the highest frequency response the device is capable of f_H , and the lowest f_L. For D.C. systems, f_L is determined by the "on time" of the instrument. f_L is a cutoff for periods longer then the time the instrument has been on. If we integrate over the instrument bandwidth we find

$$N_{1/f} = K \int (1/f)\, df = K \ln (f_H/f_L) \tag{2.15}$$

where $N_{1/f}$ is the noise power in Watts, and K is a constant of proportionality, also in Watts. The noise power per decade can be determined by substituting $f_H = 10f_L$ which yields;

$$N_{1/f} = 2.3K \text{ / decade} \tag{2.16}$$

which is independent of the decade of frequency measured. The noise power from 1Mhz to 10Mhz is the same as 0.001 to 0.0001 hertz. Each decade of noise is uncorrelated with respect to each other, so the total noise is;

$$N_{Total} = (N_1^2 + N_2^2 + N_3^2 + ...N_n^2)^{1/2} \tag{2.17}$$

where n is the number of decades of bandwidth observed. Substituting in equation 2.16 and simplifying yields;

$$N_{Total} = (n(2.3K)^2)^{1/2} = 2.3Kn^{1/2} \tag{2.18}$$

If an instrument which has D.C. to 100Hz response has been measuring for 100 seconds, it has an effective measurement bandwidth of 4 decades. If left on for 2 hours 45 minutes it will gain two more decades of bandwidth which will increase the fraction of 1/f noise by $(6/4)^{1/2} = 1.22$, or 22%. After a day of operation the increase would be 32%. If left on from the beginning of the big bang (that ought to be about the maximum practical limit!) around ten billion years ago, the 1/f noise would have increased 218% over the 100 second interval. So, 1/f noise doesn't really diverge with long measurement times, but it is important to note that it does gradually increase over longer measurement times. This is just the opposite of white noise sources which will "average out" as the square root of measurement time.

2.4.5 Amplifier Input Current Noise

All real amplifiers create input current noise, which is an RMS sum of all the noise source which acts in series with the input of the amplifier (sometimes referred to as series noise sources). For a JFET input Operational Amplifier the input impedance is very high and the series noise is dominated by Shot noise from the gate leakage current. Some JFETs have additional Flicker noise [21]. As the leakage current through the gate oxide is determined by thermally generated carriers, the input impedance is a very strong function of temperature. The resistance will approximately double for every decrease of ten degrees centigrade [50]. On Op-Amp specification sheets, the gate leakage is called Input Bias Current as a holdover from bi-polar transistors. Ignoring any flicker noise, the amplifier input current noise density is

$$i_{na} / \text{ Root Hz } = (2qI_b)^{1/2} \qquad (2.19)$$

where I_b is the input bias current to the amplifier.

2.4.6 Amplifier Input Voltage Noise

All real amplifiers create input voltage noise, which is an RMS sum of all the noise source which act in parallel with the input of the amplifier (sometimes referred to as parallel noise sources). The resistance of the channel in JFETs creates a Johnson noise voltage which is referred to the output because of its dependency on the source impedance and feedback impedance which are functions of frequency. The "gain" by which the noise voltage will get mapped onto the output depends on the ratio of these two frequency dependant functions, so the noise may be a function of a particular bandwidth in a complex way. Figures 2.3 and 2.4 show the source and feedback impedance as a function frequency for a typical Photodiode TIA design used for reference in this work. This will be discussed further in section 2.6, on summing the noise terms. As voltage noise often contains some component of 1/f noise, it is common to see voltage noise listed for a series of specific bandwidth ranges in amplifier specification sheets. In lower quality amplifiers it is the dominant source of noise below 1kHz. In high quality operational amplifiers it is generally not the limiting factor.

In circuits with high capacitance inputs (large area photodetectors) and high resistance, low capacitance feedback loops, gain peaking can occur. This results from the feedback loop shifting the phase enough to cause positive feedback into the summing junction, destabilizing the amplifier, and creating a large noise gain. For the low bandwidth applications considered here, the amount of capacitance across the feedback loop is much more than the few picofarads required to prevent gain peaking, so it is reasonable to neglect its effect in this treatise.

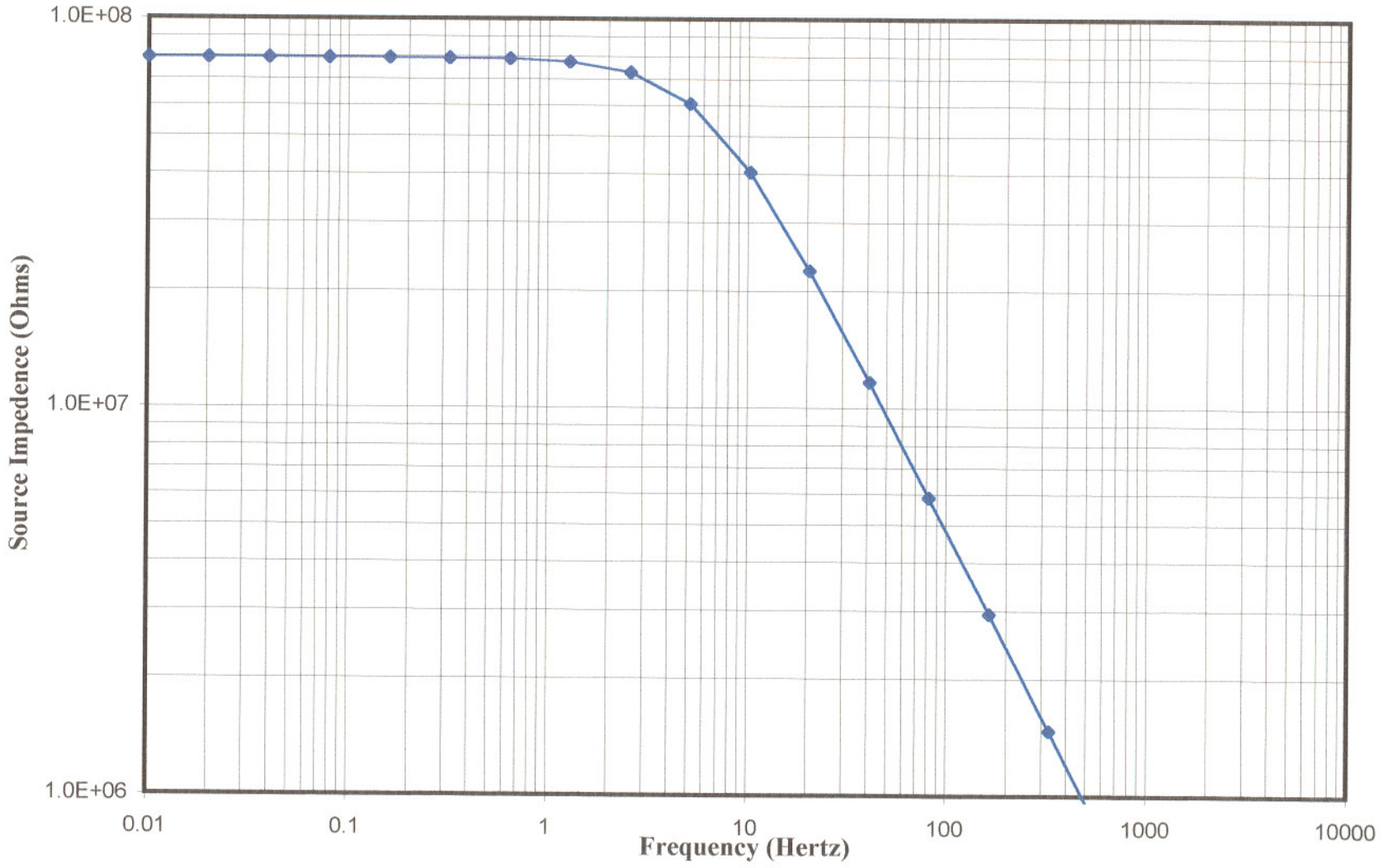

Figure 2.3 Effective Source Impedence (Equation 2.27) for the TIA Model.

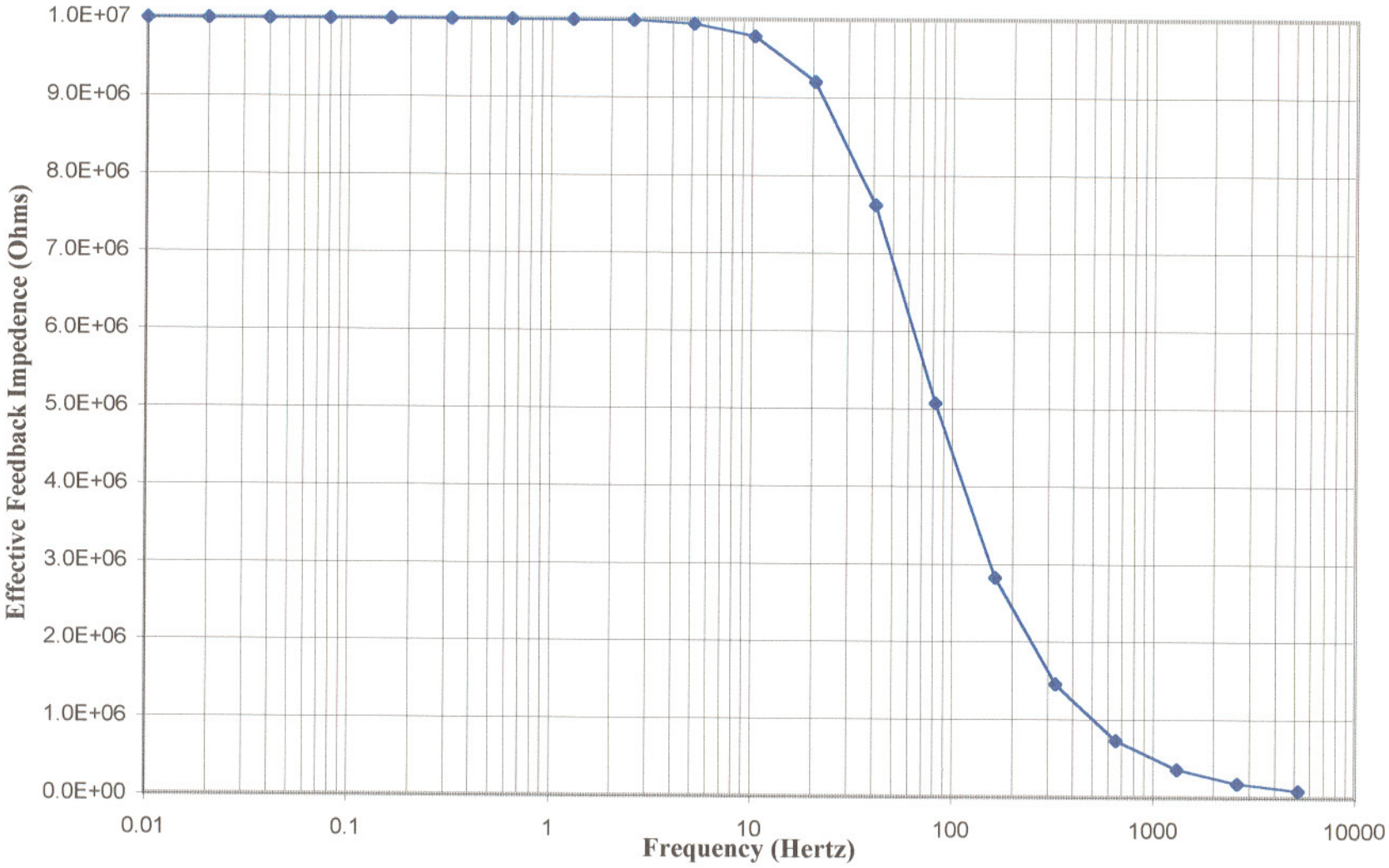

Figure 2.4 Effective Feedback Impedence (Equation 2.26) for the TIA Model.

2.4.7 Input Offset Error

Even when operational amplifiers are run in the photovoltaic mode, there is a small offset voltage which appears on the input, and therefore across the photodiode. Because this voltage is subject to thermal drift, the offset voltage can not be completely zeroed out without danger of driving the analog to digital convertor (ADC) out of range. The necessary safety margin will depend on the offset drift rate for the specific amplifier.

$$E_{os} = E_o + \Delta E_o (T_h - T_l) \tag{2.20}$$

where:

E_{os} = Offset across the photodetector (volts)

E_o = Amplifier input offset voltage (volts)

ΔE_o = Amplifier input offset voltage drift (V/°C)

T_h = Highest temperature of amplifier operation

T_l = Lowest temperature of amplifier operation

The input offset voltage maps onto the output by the effective DC gain of the transimpedance circuit. This is also the output voltage produced by the sum of the photodetector dark current and the amplifier input bias current flowing through the feedback resistor.

$$E_{oo} = E_{os} (1 + R_f / R_{sh}) = [(I_b + I_d) R_f] \tag{2.21}$$

where:

E_{oo} = Offset voltage on the output (volts)

E_{os} = Offset across the photodetector (volts)

R_f = Feedback Resistance (ohms)

R_{sh} = Photodiode shunt resistance (ohms)

I_b = Amplifier input bias current (amps)

I_d = Photodiode dark current

This small input offset voltage (generally tens of microvolts) creates a dark current through the photodetector that generates a Shot noise density of:

$$i_{no}/rh = (2qI_d)^{1/2} \tag{2.22}$$

2.5 Addition of noise sources

When noise sources are generated independent of each other, and there is no relationship between their instantaneous values, they are uncorrelated. If they are of the same frequency and phase, they are correlated and will add together arithmetically. Mixing of correlated and uncorrelated sources will result in partially correlated noise, and they will add in general;

$$N^2 = N_1^2 + N_2^2 + 2CN_1N_2 \tag{2.23}$$

where C is the correlation coefficient and ranges between 1 and -1. When C equals one, the noise is totally correlated, and the RMS values of the noise add together. For C equal to minus one, the noise terms are one hundred percent correlated, but out of phase, so they cancel each other out. When C is zero, they are fully uncorrelated and add by the square root of the sum of the squares.

Correlated noise sources can originate in circuits of interest from jitter and timing

issues which are an important, but often neglected, side effect of software architecture. Other extrinsic sources like 60hz or digitally induced noise might be correlated. The maximum calculation error caused by incorrectly assuming that noise sources are uncorrelated is generally not very great. As an example, if N_1 equals N_2 for C equal zero; total noise equals the square root of two times the individual level. If C equals unity, the total noise is twice the individual level, which is only 30% different.

2.6 Summing the Noise Terms

As mentioned in the earlier section, the various noise terms originate from independent sources and the total input spectral noise density referred to the input is calculated by summing the squares of the individual RMS values. Thus, we must sum the Shot noise from photo-generated currents (Eq 2.5), Shot noise from thermally generated currents in the photodetector (Eq 2.10), Johnson noise from the photodiode shunt resistance (Eq 2.13), Johnson noise from the feedback resistor (Eq 2.13), amplifier input current noise (Eq 2.19), Shot noise from photodiode dark current (Eq 2.22), and any 1/f noise if appropriate (Eq 2.14).

$$I_t^2/RHz = 2\eta QA_d q + 4kT_d/R_{ideal} + 4kT_d/R_s + 4kT_f/R_f + 2qI_b + 2qI_d + kI_B^{\alpha}/f^{\beta} \qquad (2.24)$$

As the ideal thermally generated Shot noise is in parallel with the leakage resistance Johnson noise and are combined in one measurement known as the shunt resistance, they add to form one term (Eq 2.11) which reduces to equation 2.25 as follows.

$$I_t^2/RHz = 2\eta QA_d q + 4kT_d/R_{sh} + 4kT_f/R_f + 2qI_b + 2qI_d + kI_B^{\alpha}/f^{\beta} \qquad (2.25)$$

The advantage of referencing noise current terms to the input is that they are in unmodified magnitudes and it is more intuitive to think about them before they are

transferred to voltage by transimpedance gain which depends on the specific circuit construction. The amplifier input voltage noise is not included in the above input current terms. It is traditionally referenced to the output because of the frequency dependent relationship to the transimpedance circuit. The feedback impedance Z_f, is defined by the following relation with frequency f: [52]

$$Z_f = R_f / [(1+2\pi f C_f R_f)^2]^{1/2} \qquad (2.26)$$

The source impedance Z_s as a function of frequency is described as follows:

$$Z_s = R_{sh} / [(1+2\pi f C_f R_{sh})^2]^{1/2} \qquad (2.27)$$

The total noise present with respect to the output of the photodiode - transimpedance combination is approximated by:

$$e_{nT} = Z_f [(N_{ea} / Z_s)^2 + i_{na}^2 + i_{np}^2 + i_{nf}^2 + i_{no}^2]^{1/2} \qquad (2.28)$$

where:

Z_f (Eq. 2.26); N_{ea} (Table 2.1); Z_s(Eq. 2.27); i_{na}(Eq. 2.19); i_{np}(photodiode noise per Eq. 2.11); i_{nf}(feedbak resistance noise per Eq 2.12); and i_{no}(Eq 2.22).

2.7 Experimental Results

2.71 Evaluating the Noise Model with Specific Parameters

Values were entered into the spreadsheet noise model for the amplifier and feedback network, photodiode, and optical throughput. Information was obtained for the Burr-Brown OPA111BM operational amplifier and the Hammamatsu 1337-66B photodetector from the manufacturers specification sheets (52,53). Temperature dependency equations were obtained from the Burr-Brown and EG&G applications notes (54,55). Optical throughput was determined as a function of measured temperature by integrating the Planck equation for blackbody radiation, the optical wavelength selective filter, and the photodiode responsivity with respect to wavelength. This model is based on the Accufiber Model 100 because good performance data is available [56,57]. An aperture correction and small spectral calibration term were determined by measurements in a blackbody calibration furnace. A table of photodiode signal currents as a function of measured wavelength was then entered into the spreadsheet. The following four tables are a summary of input data for the amplifier (Table 2.1), the photodiode (Table 2.2), and optical throughput (Table 2.3) and the physical constants (Table 2.4).

The left side of Eq. 2.28 is graphed out in Figure 2.5. It is obvious from this graph that very little noise is contributed by frequencies higher than 1 kHz, primarily a result of the 330 pF capacitance in the feedback loop. The feedback and diode impedances were plotted in Figures 2.3 and 2.4 respectively. The various components that make up the total voltage noise referred to the output are plotted in Figure 2.6. It is interesting to note that even though the amplifier voltage noise increases with frequency, it can not override the high frequency noise suppression that results from the feedback capacitance. In general the amplifier voltage noise is the leading contributor to noise in wide bandwidth circuits used in the communications industry, but as can be seen it is not a significant contributor in these

low frequency applications. Figure 2.7 displays the total noise components for varying bandwidths with a low frequency limit of 0.01 hertz. This plot was created by integrating equation 2.28 over different bandwidths. It is clear that for bandwidths above 1 kHz the amplifier voltage noise dominates and at bandwidths below 1 kHz the Johnson noise in the feedback resistor dominates. All other contributions to noise have an insignificant effect to the total values in this particular embodiment of the transimpedance amplifier - photodiode design.

Figure 2.8 shows the relationship between signal and noise voltage (referred to the output) as a function of measured temperature. A signal bandwidth of 76 Hz was used to match the Model 100 characteristics. The signal to noise ratio equaled 1.0 at 340°C with a noise voltage floor of about 50 microvolts rms. Although quantitave data was not available for these parameters, they are reasonable for this configuration.

Now that it has been demonstrated that the amplifier voltage noise is insignificant in this analysis, it is appropriate to express the verious noise terms as currents referred to the input. This allows for a more direct computation of noise by use of the fundamental equations (Shot and Johnson noise) without concern of the characteristics of the amplifier effective gain and frequency response. Figure 2.9 shows the input signal photocurrent with its related noise terms as a function of measured temperature. This graph is expressed as a noise current density from equation 2.25, so the values have been normalized to a one hertz bandwidth. Figure 2.10 in an expansion of Figure 2.9 to show more detail on the various noise components, and the signal current has been omitted. From these graphs it can be clearly seen that even though the Johnson noise from the feedback resistor is the dominate noise source below 500°C, the photodiode noise terms are not too far below it. Therefore, if the feedback noise were removed, consideration must be given to the photodiode noise inorder to gain dramatic improvements.

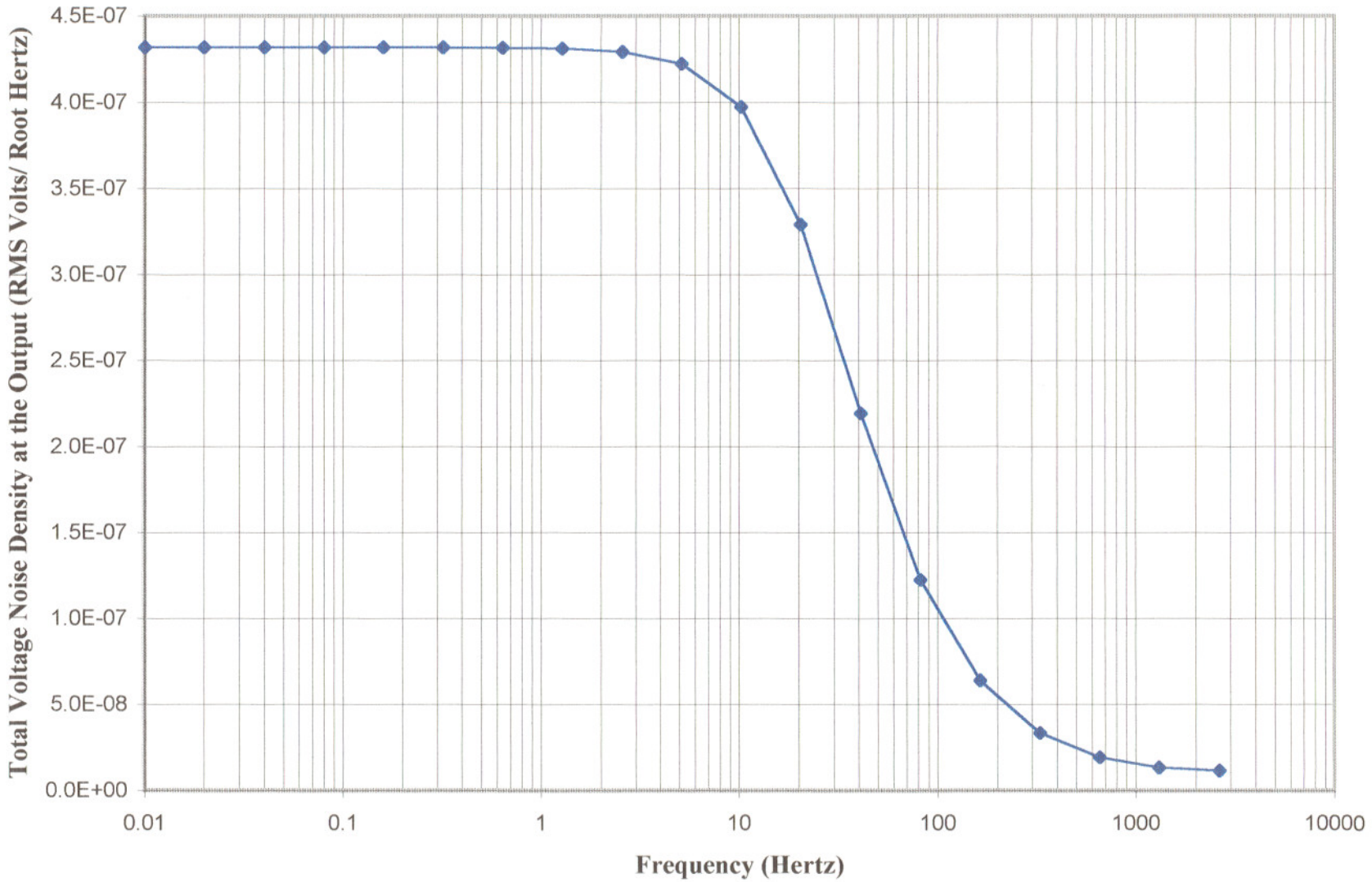

Figure 2.5 Total Noise Voltage Spectral Density (Equation 2.28) refered to the Output- TIA Model.

Table 2.1 Transimpedance Amplifier Data Table

Description	Symbols	Value	Units
Feedback Resistor Resistance	R_f	1.00E+07	Ohms
Feedback Capacitance	C_f	3.30E-10	Farads
Feedback Resistor Operating Temperature	T_f	300	Kelvin
Temperature of Amplifier Specifications	T_r	300	Kelvin
Temperature of Amplifier Operation	T_a	300	Kelvin
Temperature of Amplifier Operation (Highest)	T_h	32	°C
Temperature of Amplifier Operation (Lowest)	T_l	20	°C
Amplifier Input Current Noise*	N_{ia}	4.00E-16	$A/Hz^{1/2}$
Amplifier Input Voltage Noise	N_{ea}	1.10E-08	$V/Hz^{1/2}$
Amplifier Input Offset Voltage	E_o	5.00E-06	V
Amplifier Input Offset Voltage Drift	$DE_o(T)$	1.00E-06	V/°C
Amplifier Input Bias Current (@T_r)	I_{bs}	7.50E-13	Amps
Amplifier Input Impedance	R_{in}	1.00E-13	Ohms
Amplifier Input and Stray Capacitance	C_a	1.00E-12	Farads
1/f Noise Linear Coefficient	k_f	1.00E-16	none
1/f Noise Current Exponential Coefficient	a	1	none
1/f Noise Frequency Exponential Coefficient	b	1	none
Op Amp Unity Gain Bandwidth	F_{un}	2.00E+06	Hertz

Table 2.2 Photodiode Data Table

Description	Symbols	Value	Units
Photodiode Capacitance	C_d	3.80E-10	Farads
Temperature of Photodiode Specifications	T_{pr}	298	Kelvin
Temperature of Photodiode Operation	T_{pa}	300	Kelvin
Photodiode Impedance from specs.	R_{ss}	1.00E+08	Ohms
Photodiode Saturation Current Temperature Exponent	S	3	None
Photodiode Emission Coefficient	N	1	None
Photodiode Energy Gap	E_g	1.11	eV
Photodiode Temperature Coefficient (1)	k_T	1.15	$°C^{-1}$
Photodiode Responsivity at Effective Wavelength	R	0.6	Amps/ Watt
Photodiode Area	A_d	32.5	mm^2
Photodiode Quantum Efficiency at Effective Wavelength	η	0.79	none

Table 2.3 **Optical Data Table**

Description	Symbols	Value	Units
Effective Wavelength(s)	W	0.95	μm
Radiant Photon Incidence	Q	*	$p/mm^2/s$
System Clear Aperture	A_c	*	mm^2
System Numeric Aperture	N.A.	.37	None
Target Temperature (Maximum)	T_{max}	1573	Kelvin
Target Temperature (Minimum)	T_{min}	473	Kelvin
Target Emissivity	e	1	None
Upper Bandwidth (Maximum Frequency)	f_u	1000	Hertz
Lower Bandwidth (Minimum Frequency)	f_l	0.01	Hertz
Total Bandwidth (fu - fl)	B	999.99	Hertz

* Values not used in this model

Table 2.4 **Physical Constants Table**

Description	Symbols	Value	Units
Planck's Constant	h	6.63E-34	Joule-sec
Velocity of Light	c	3.00E+08	Meters/Sec
Electric Charge	q	1.60E-19	Coulomb
Boltzmann's Constant	k	1.38E-23	Joules/ °K
First Radiation Constant = $2\pi hc^2$	C_1	3.7418E-16	$Watt*\mu m^2$
Second Radiation Constant = hc/k	C_2	14387.7	μm*°K

Table 2.5 Table of Calculated Constants and Terms for the TIA

Description	Symbols	Value	Units
Calculated Total Amplifier Offset with Drift Voltage	E_{ot}	0.000017	Volts
Shot Noise from Photon Generated Carriers (Signal)	i_{nsig}	Figure 2.9 Eq 2.5	Amps/RHz
Johnson Noise in the Feedback Resistor	i_{nf}	4.0704E-14	Amps/RHz
"Johnson Noise" in the Photodiode	i_{np}	1.4448E-14	Amps/RHz
Calculated Nia from Input Bias Current Shot Noise	i_{na}	4.902E-16	Amps/RHz
Photodiode Shot Noise from Amplifier Offset Voltage	i_{no}	2.6196E-16	Amps/RHz
Amplifier 1/f Noise	$i_{n1/f}$	*	Amps/RHz
Source Impedance	Z_s	Figure 2.3	Ohms
Feedback Impedance	Z_f	Figure 2.4	Ohms
Total Voltage Noise on Output of PD-TIA combination	e_{nT}	Figure 2.8 Eq 2.28	Volts/RHz
DC Noise Gain (1+Rf/Rsh)	G_{dc}	1.126	1
Onset of Noise Gain	F_z	25.24	Hertz
High Frequency Noise Gain	G_{hf}	2.152	1
Beginning of Noise Gain Plateau and Signal Gain Rolloff	F_p	48.23	Hertz

Table 2.5 Table of Calculated Constants and Terms for the TIA (Continued)

Description	Symbols	Value	Units
Beginning of Noise Gain Rolloff	F_{nc}	9152	Hertz
Signal Bandwidth (3 dB Brickwall)	BW_{sig}	75.76	Hertz
Noise Bandwidth (3 dB Brickwall)	BW_{nos}	14376	Hertz
Voltage Output Noise from Current Sources - Sig Shot	e_{ni}	3.7597E-06	Volts
Total Voltage Noise on Output due to Voltage Sources	e_{nv}	2.8377E-06	Volts
Total Voltage Noise on Output - Sig Shot	e_{nT2}	4.7104E-06	Volts
Photodiode Operating Impedance (Shunt Resistance)	R_{sh}	79370052.6	Ohms
Amplifier Input Bias Current (@Ta)	I_b	7.5E-13	Amps

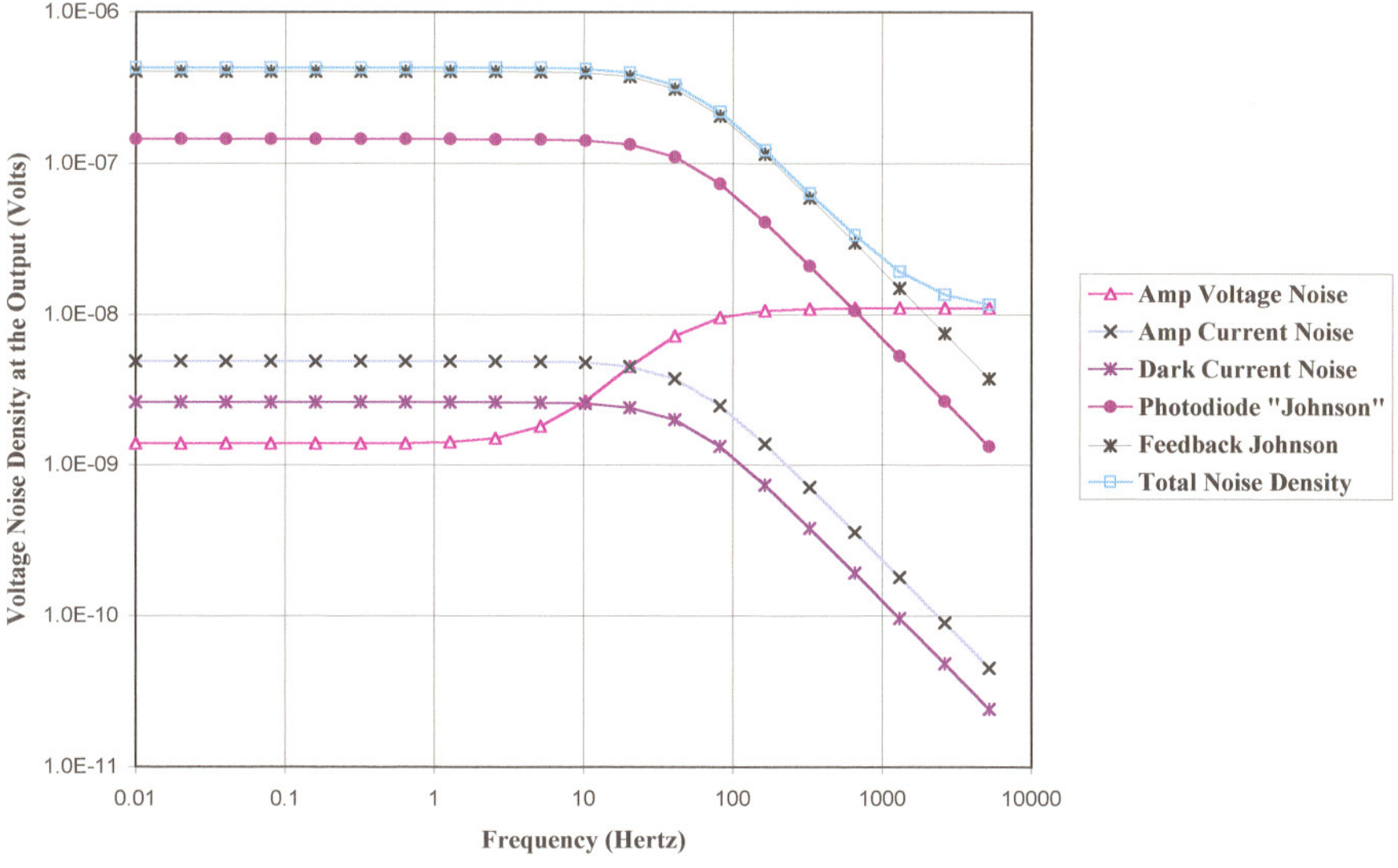

Figure 2.6 Components of Total Noise Voltage Spectral Density (Equation 2.28) for the TIA Model.

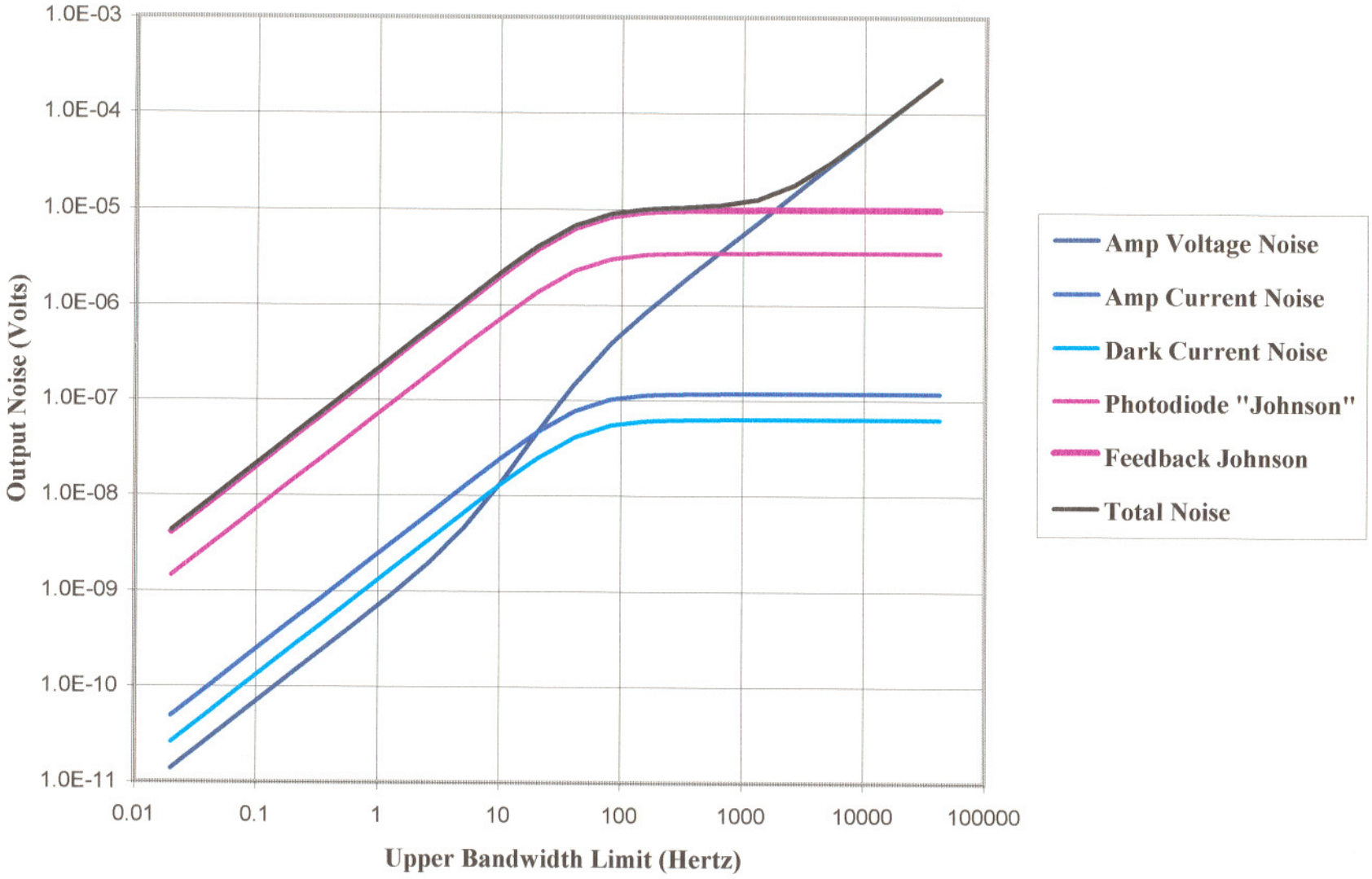

Figure 2.7 Total Noise Voltage as a Function of Bandwidth. For the TIA Model and Lower Bandwidth Limit of 0.01 Hertz

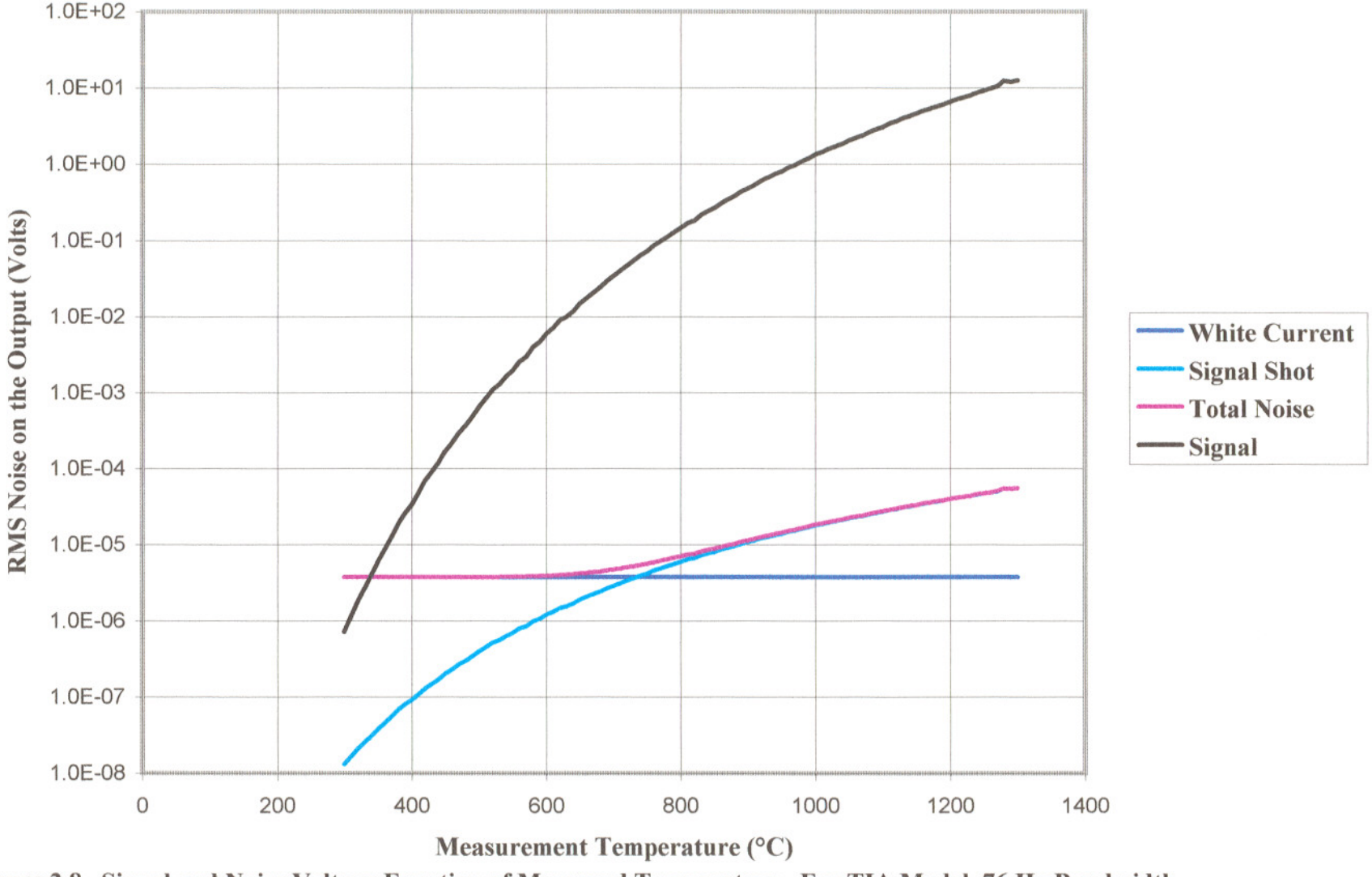

Figure 2.8 Signal and Noise Voltage Function of Measured Temperature. For TIA Model, 76 Hz Bandwidth, Referenced to the Output.

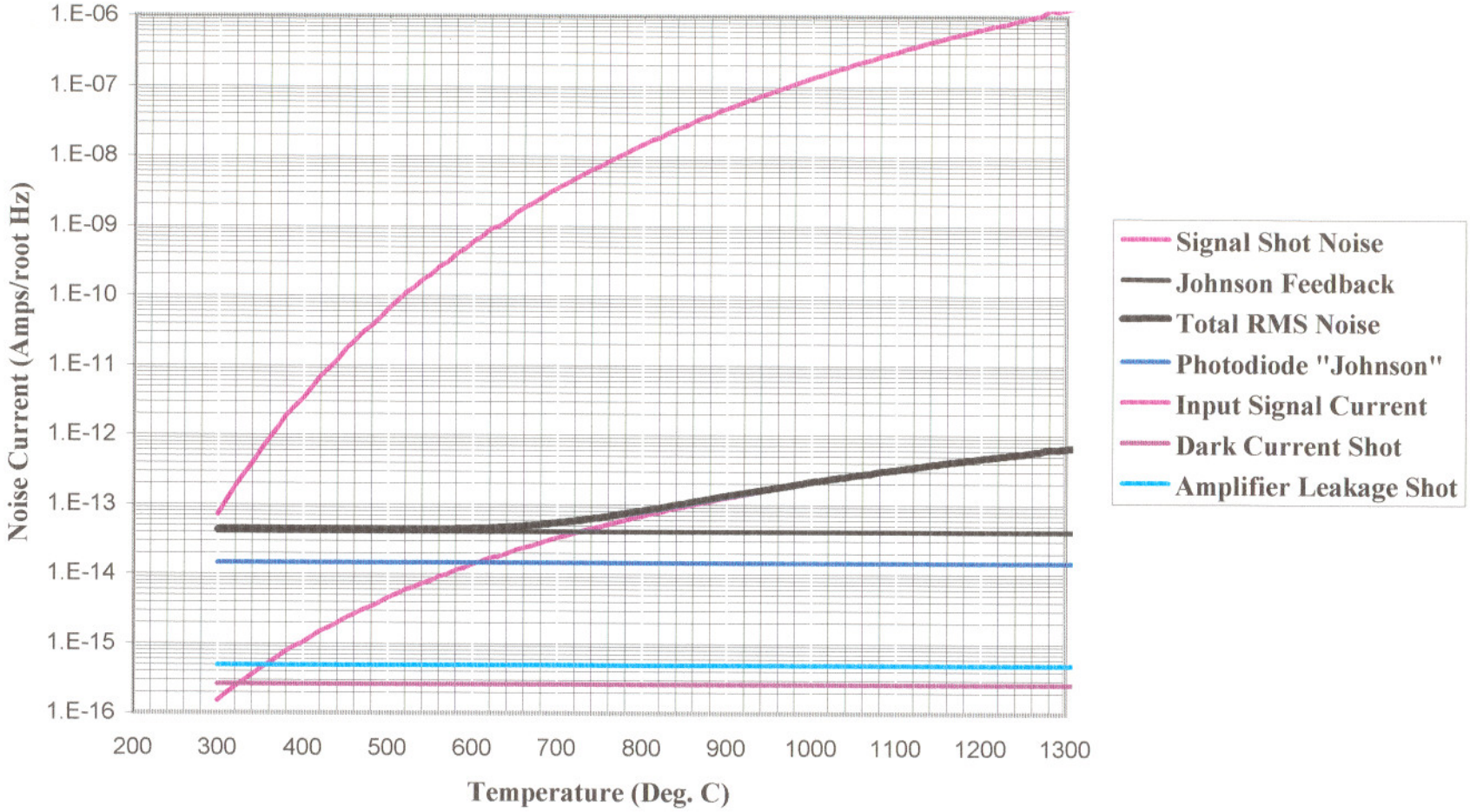

Figure 2.9 Input Signal Current with Related Terms as a Function of Measured Temperature. For the TIA Model - Equation 2.25

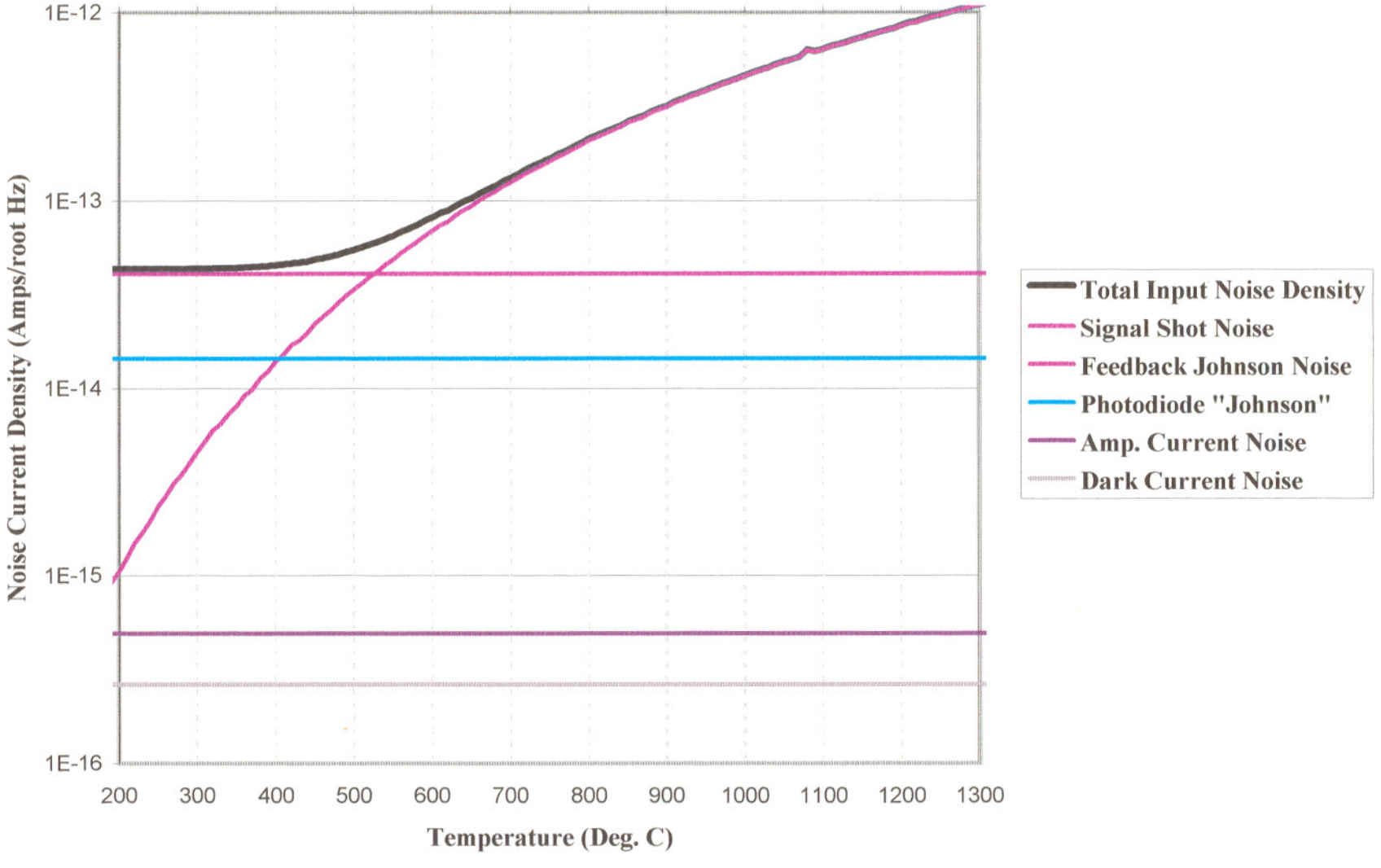

Figure 2.10 Components and Sum of Input Current Noise Density. For the TIA Model - Equation 2.25

The input summarized in the above tables generated output listed in Table 2.5, and Figures 2.5 to Figure 2.12. These results will be discussed in Sections 2.72 and 2.73. Source and feedback impedances, noise voltage on the output, and photon generated Shot noise are plotted as a function of frequency in Figures 2.3, 2.4, 2.8, 2.9 respectively.

2.72 Checking the Model - Resolution vs Measured Temperature

The $2\eta QA_d q$ term in the total noise equation (Eq 2.25), which represents the photon generated current in the photodetector, was determined by integrating the Planck equation times the filter transmission curve (950nm center wavelength, 70nm Full Width at Half Maximum) times the photodetector responsivity. Aperture corrections and slight spectral calibration factor were determined empirically. These measurements were made by inserting a 12" long 0.050" diameter single crystal sapphire lightpipe into a precision blackbody calibration furnace. The radiance from the lightpipe transferred to the detector assembly through a three meter long, 600 micrometer diameter high numeric aperture fused silica fiberoptic cable, where it was filtered and focused onto the photodetector. The blackbody furnace was calibrated by a NIST traceable type S thermocouple (+- 0.2% @1000°C accuracy). Photodiode currents were precisely related to temperature. As the blackbody calibration furnace can be controlled to within 30 milliKelvins, the rms noise of the detection system can be easily determined as a function of measurement temperature.

Figure 2.11 is a graph of the photon generated currents (signal) divided by total noise current referred to the input as a function of measured temperature. These values were generated for a one hertz bandwidth and demonstrate a S/N of one at 290°C. This S/N data can be converted to temperature measurement resolution by use of equations 1.0 and 1.3 and is graphed in Figure 2.12. Data from Accufiber Inc. application notes [56], and a European

standards laboratory [57] are plotted along with the models predicted values. Data points for higher temperature were not plotted as the instrument resolution is limited by the ADC in these region and not by the noise in the detection circuitry. The theoritical model agrees well with the measured data, accurately predicting the rapid decrease in temperature resolution below 500°C

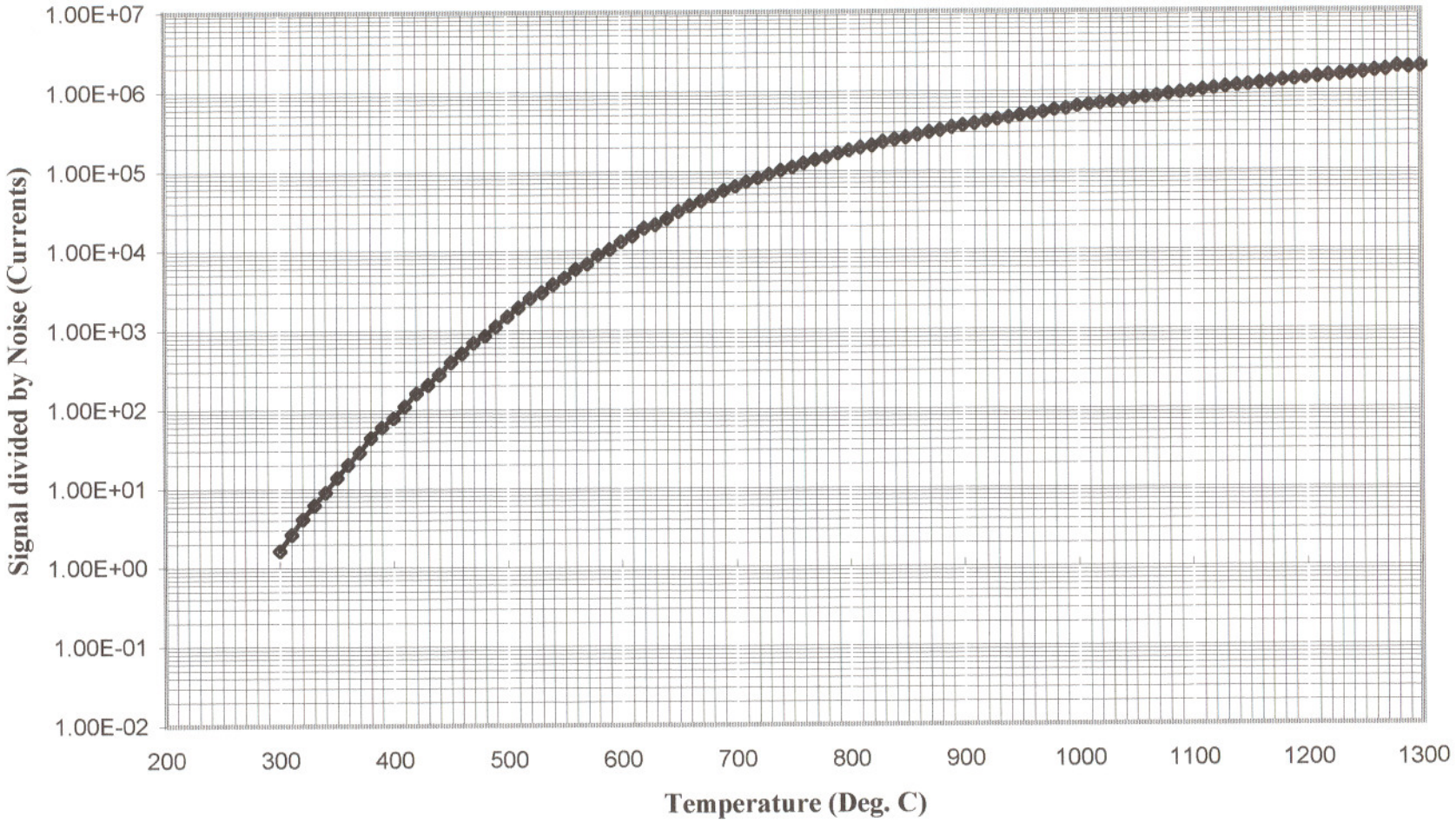

Figure 2.11 Signal divided by Total Noise. For the TIA Model, Currents refered to the Input.

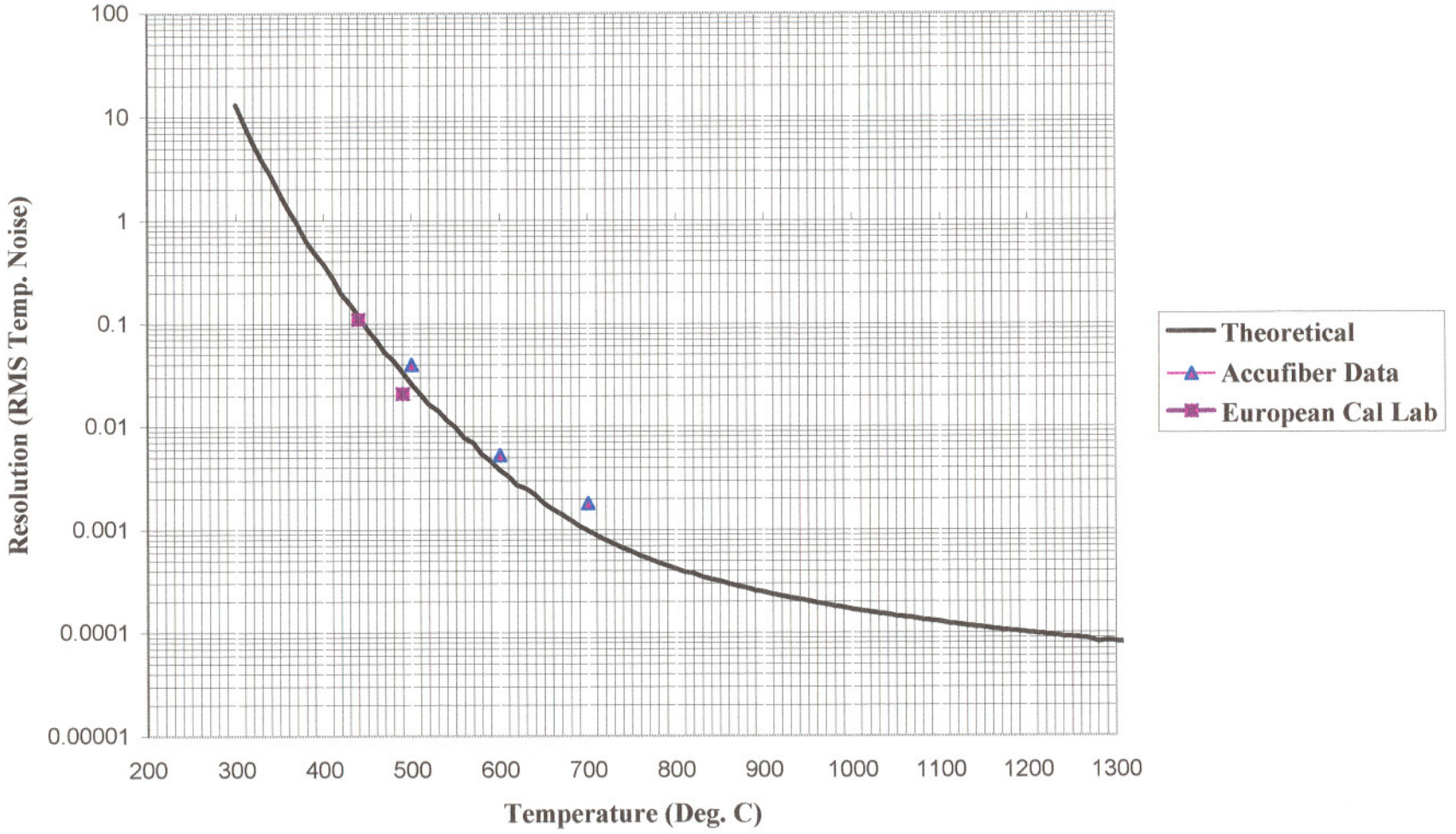

Figure 2.12 Resolution of Temperature as a Function of Temperature Measured at 1 Hertz Sample Rate (for the TIA Model).

2.73 The Effect of Lowering Temperature on Noise in a TIA

As can be observed from Figure 2.10 the Johnson noise in the feedback resistor determines the noise floor for temperature measurements below 525°C (10^{-9} Amps signal current) for frequencies below 1kHz. The Johnson noise is proportional to the square root of absolute resistor temperature and would require drastic decreases in temperature to effect any major decrease in noise. For example, to decrease the Johnson noise of a resistor operating at room temperature (300K) one order of magnitude would require reducing the temperature to 3K. This is certainly not a practical solution for industrial instrumentation. A modest change of operating temperature from 22°C ambient to 0°C would affect the resolution of a 300°C measured temperature by only a 0.4°C RMS decrease in noise (13°C to 12.6°C).

2.8 Chapter Summary

This chapter developed the background information required to analysis the intrinsic electrical noise floor in photodiode / transimpedance circuits. Each of the noise sources inherent in this circuit has been identified, and quantified. A mathematical model was developed to predict total circuit noise of a specific industrial system and its limit to temperature measurement resolution. Experimental conformation of the predicted values was presented. This model calculated that resolution was limited primarily by Johnson noise in the feedback resistor and was not strongly dependent on ambient temperature. In the following chapter this model will be used to estimate the intrinsic noise floor in a switched integrator circuit and the overall effect that ambient temperature plays on each component of the system.

CHAPTER 3

Modifying the Model for a Slightly Cooled Integrating Detector (SCID)

3.1 The Experimental Design for a SCID

As mentioned in the introduction, the basic concept of the SCID is to replace the resistive term in the feedback loop with and integrating capacitor, virtually eliminating the limiting Johnson noise floor. The remaining noise currents are dependent upon thermally generated carriers, which are highly temperature dependant and can be substantially reduced by slight cooling (23 degrees °C in this example) both the amplifier and the photodiode. The Burr-Brown AFC2101 switched integrator is a monolithic device, with very high quality internal integrating capacitor, and matched switches which reduce charge injection to nearly zero. The same photodetector was used as in our reference TIA design, the Hammamatsu S1337BM, which is known for its stability and high dynamic impedance. The control logic was regulated by a PIC microprocessor, because they are fast, inexpensive, and have more then enough functions for this simple control environment. The photodetector and integrator were mounted on a two stage thermoelectric cooler (TEC), which was set to control the

temperature at 2 degrees above freezing to avoid moisture condensing onto the optics. A small amount of heat from the output of the TEC was allowed to flow to the input window of the detector to assure a condensation free optical path. Control changes to the TEC were synchronized with the integrator control logic to avoid inductive switching noise from the cooler. The signal output from the integrator was amplified, digitized, mapped into the temperature domain, and transferred through RS232 for storage and analysis.

3.2 Modifying The Model for a SCID.

Noise data for low input current operation of the ACF2101BM is not available from Burr-Brown. Input bias current as a function of temperature is published in the application notes along with a very brief description of the components of total output voltage noise. These noise sources are not related to fundamental mechanisms, but are referred to as Integrate noise, Hold noise, and Reset noise. These are the noise terms for the three modes of the ACF2101 operation. Both Hold noise and Reset noise are listed as a constant 10μV rms each. The Integrate noise is given as;

$$e_{nI} = (10\mu Vrms)*(1+ C_d / C_f) \qquad (3.1)$$

This term looks like the input voltage noise times the DC voltage gain of the system. The Hold mode was not used in the configuration evaluated in this study, so the 10μV rms of Reset noise adds in quadrature to the 48μV rms of Integrate noise to yield a 49μV rms noise floor below 1Hz. The model uses the EG&G equations [55] for mapping input voltage noise onto the output, and includes the frequency dependent Z_s (Figure 3.1) and Z_f (Figure 3.2) terms, which give higher and probably more realistic values because of "Noise Boosting" effects. As little electrical information on the input amplifier for the AFC2101 is available, needed parameters for the model were "borrowed" from the OPA111BM which

is also a JFET amplifier based on Burr-Brown's exclusive low noise, low leakage technology. Using these numbers for and uncooled integrator the model predicted the input voltage noise term will dominate for all bandwidths and yielded a value of 48 μV rms for bandwidths less than 1 hertz. This probabily explains why the voltage noise specifications are the only noise parameters given by the manufacture.

There is no mention of temperature dependance of these noise terms in the specifications, but measurements were made at 0°C and the total output voltage noise was determined to be less than 0.25μV peak to peak with a 20 second integration time. This should be equivalent to about 0.16μVrms at 1Hz which demonstrates the very large temperature dependance of these noise terms.

3.3 Predicting the Effects of Cooling in a SCID.

The following input data table 3.1 for the switched integrating amplifier shows the electrical characteristics used in the model for the cooled configuration. The photodiode table, optical throughput table, and the physical constants table are identical to those for the TIA with the obvious exceptions of operating temperatures and some corrections for throughput and will not be repeated .

Table 3.1 Switched Integrating Amplifier Data Table

Description	Symbols	Value	Units
Feedback Resistor Resistance	R_f	1.00E+12	Ohms
Feedback Capacitance	C_f	1.00E-10	Farads
Feedback Resistor Operating Temperature	T_f	275	Kelvin
Temperature of Amplifier Specifications	T_r	300	Kelvin
Temperature of Amplifier Operation	T_a	275	Kelvin
Temperature of Amplifier Operation (Highest)	T_h	32	°C
Temperature of Amplifier Operation (Lowest)	T_l	20	°C
Amplifier Input Current Noise*	N_{ia}	4.00E-16	$A/Hz^{1/2}$
Amplifier Input Voltage Noise	N_{ea}	1.10E-08	$V/Hz^{1/2}$
Amplifier Input Offset Voltage	E_o	5.00E-06	V
Amplifier Input Offset Voltage Drift	$DE_o(T)$	1.00E-06	V/°C
Amplifier Input Bias Current (@T_r)	I_{bs}	7.50E-13	Amps
Amplifier Input Impedance	R_{in}	1.00E-13	Ohms
Amplifier Input and Stray Capacitance	C_a	1.00E-12	Farads
1/f Noise Linear Coefficient	k_f	1.00E-16	none
1/f Noise Current Exponential Coefficient	a	1	none
1/f Noise Frequency Exponential Coefficient	b	1	none
Op Amp Unity Gain Bandwidth	F_{um}	2.00E+06	Hertz

3.4 Experimental Results, RMS Noise & Offset

The input summarized in the Table 3.1, Tables 2.2, 2.3, 2.4 generated output listed in Table 3.2 for the uncooled design and Table 3.3 for the system cooled to 2°C.

Table 3.2 Table of Calculated Constants and Terms for the Uncooled Switched Integrator

Description	Symbols	Value	Units
Calculated Total Amplifier Offset with Drift Voltage	E_{ot}	0.000017	Volts
Shot Noise from Photon Generated Carriers (Signal)	i_{nsig}	Figure 3.6	Amps/RHz
Johnson Noise in the Feedback Resistor	i_{nf}	4.0704E-14	Amps/RHz
"Johnson Noise" in the Photodiode	i_{np}	1.4448E-14	Amps/RHz
Calculated Nia from Input Bias Current Shot Noise	i_{na}	4.902E-16	Amps/RHz
Photodiode Shot Noise from Amplifier Offset Voltage	i_{no}	2.6196E-16	Amps/RHz
Amplifier 1/f Noise	$i_{n1/f}$	*	Amps/RHz
Source Impedance	Z_s	Figure 3.1	Ohms
Feedback Impedance	Z_f	Figure 3.2	Ohms
Total Voltage Noise on Output of PD-TIA combination	e_{nT}	Fig. 3.3 - 3.6	Volts/RHz Volts
DC Noise Gain (1+Rf/Rsh)	G_{dc}	1.126	1
Onset of Noise Gain	F_z	25.24	Hertz
High Frequency Noise Gain	G_{hf}	2.152	1

Table 3.2 Table of Calculated Constants and Terms for the Uncooled Switched Integrator (Continued).

Description	Symbols	Value	Units
Beginning of Noise Gain Plato and Signal Gain Rolloff	F_p	48.23	Hertz
Beginning of Noise Gain Rolloff	F_{ne}	9152	Hertz
Signal Bandwidth (3 dB Brickwall)	BW_{sig}	75.76	Hertz
Noise Bandwidth (3 dB Brickwall)	BW_{nos}	14376	Hertz
Voltage Output Noise from Current Sources - Signal Shot	e_{ni}	3.7597E-06	Volts
Total Voltage Noise on Output due to Voltage Sources	e_{nv}	2.8377E-06	Volts
Total Voltage Noise on Output - Sig Shot	e_{nT2}	4.7104E-06	Volts
Photodiode Operating Impedance (Shunt Resistance)	R_{sh}	79370052.6	Ohms
Amplifier Input Bias Current (@Ta)	I_b	7.5E-13	Amps

Table 3.3 Calculated Constants and Terms for the Switched Integrator Cooled to 2°C

Description	Symbols	Value	Units
Calculated Total Amplifier Offset with Drift Voltage	E_{ot}	0.000017	Volts
Shot Noise from Photon Generated Carriers (Signal)	i_{nsig}	Figure 3.6	Amps/RHz
Johnson Noise in the Feedback Resistor	i_{nf}	4.0704E-14	Amps/RHz
"Johnson Noise" in the Photodiode	i_{np}	1.4448E-14	Amps/RHz
Calculated N_{ia} from Input Bias Current Shot Noise	i_{na}	4.902E-16	Amps/RHz
Photodiode Shot Noise from Amplifier Offset Voltage	i_{no}	2.6196E-16	Amps/RHz
Amplifier 1/f Noise	$i_{n1/f}$	*	Amps/RHz
Source Impedance	Z_s	Graph	Ohms
Feedback Impedance	Z_f	Graph	Ohms
Total Voltage Noise on Output of PD-TIA combination	e_{nT}	Fig. 3.3 - 3.6	volts/RHz Volts
DC Noise Gain (1+Rf/Rsh)	G_{dc}	1.126	1
Onset of Noise Gain	F_z	25.24	Hertz
High Frequency Noise Gain	G_{hf}	2.152	1

Table 3.3 Calculated Constants and Terms for the Switched Integrator Cooled to 2°C (Continued).

Description	Symbols	Value	Units
Beginning of Noise Gain Plato and Signal Gain Rolloff	F_p	48.23	Hertz
Beginning of Noise Gain Rolloff	F_{ne}	9152	Hertz
Signal Bandwidth (3 dB Brickwall)	BW_{sig}	75.76	Hertz
Noise Bandwidth (3 dB Brickwall)	BW_{nos}	14376	Hertz
Voltage Output Noise from Current Sources - Sig Shot	e_{ni}	3.7597E-06	Volts
Total Voltage Noise on Output due to Voltage Sources	e_{nv}	2.8377E-06	Volts
Total Voltage Noise on Output - Sig Shot	e_{nT2}	4.7104E-06	Volts
Photodiode Operating Impedance (Shunt Resistance)	R_{sh}	79370052.6	Ohms
Amplifier Input Bias Current (@Ta)	I_b	7.5E-13	Amps

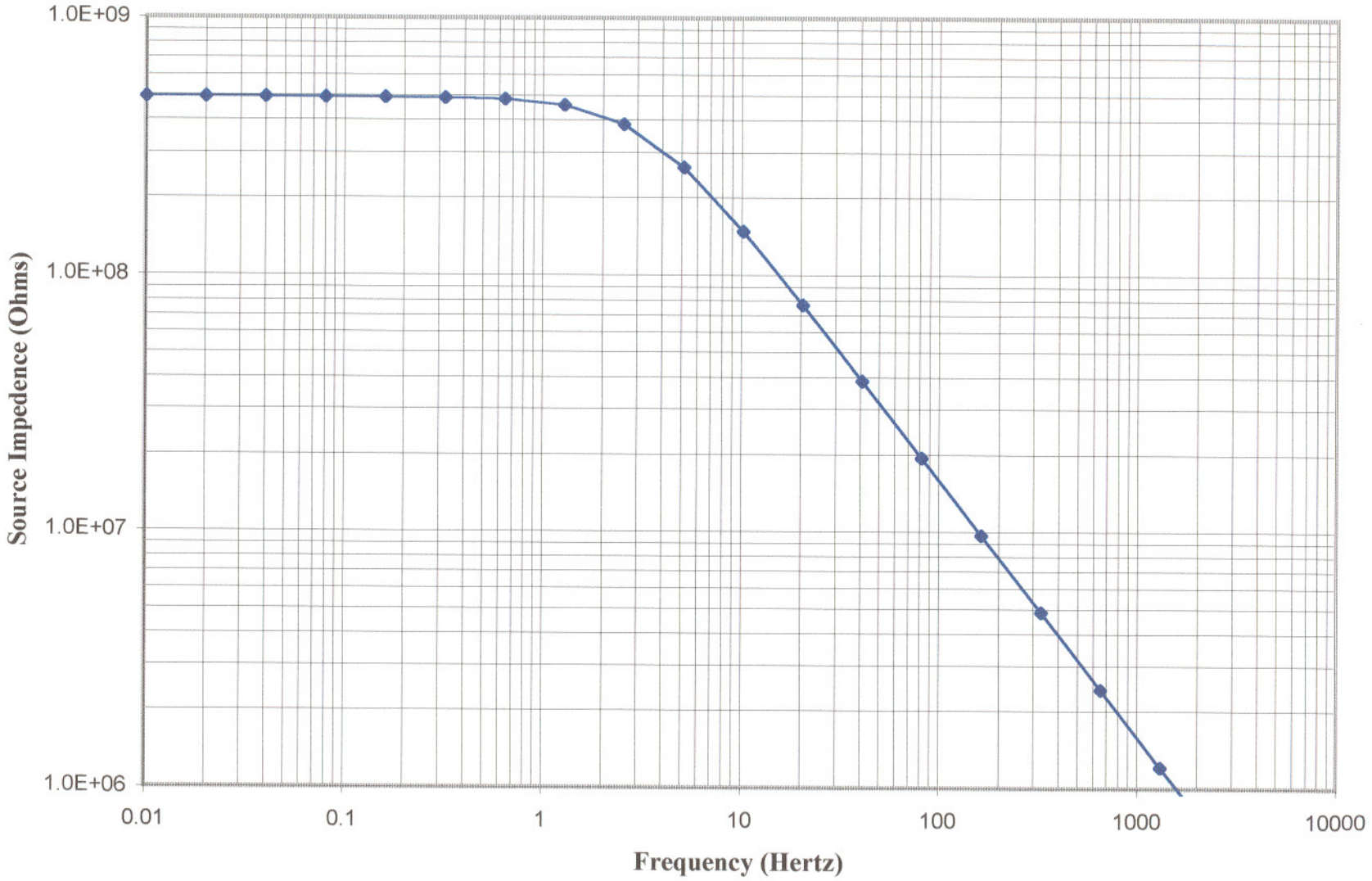

Figure 3.1 Effective Source Impedence for the SCID Model (Equation 2.27).

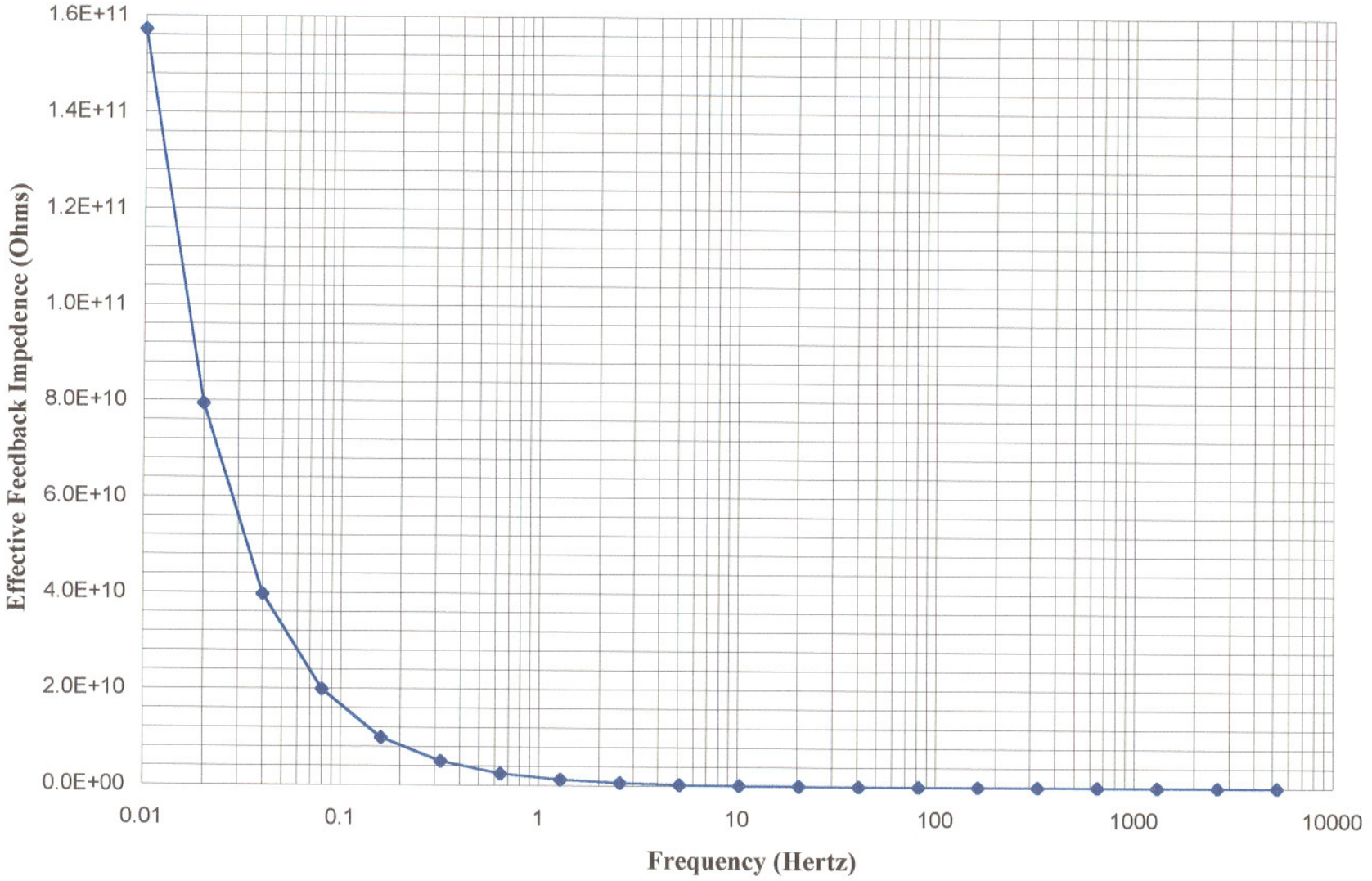

Figure 3.2 Effective Feedback Impedence for the SCID Model (Equation 2.27)

The basic analysis of the SCID is the same used for the TIA which allows for a direct comparison of performance properties. Figure 3.1 is a graph of the source impedance (Eq 2.27) and reflects the changes expected of using a smaller photodiode i.e. smaller capacitance (greater bandwidth) and higher leakage resistance.

By replacing the feedback resistor with a capacitor, the only resistive element left in the feedback loop is the capacitor leakage resistance. The RC time constant becomes huge as reflected in Figure 3.2 which was generated from Eq 2.27.

As can be seen from the total noise voltage spectral density (Figure 3.2, generated from Eq 2.28), the noise bandwidth has been reduced by three orders of magnitude. A more detailed look is presented in Figure 3.4 which graphs the individual terms (right hand side of equation 2.28) of the noise voltage spectral density. As in the TIA design, noise is limited above 1 kHz by the amplifier voltage noise, but below 1 kHz it is limited by the photodiode noise rather than the feedback Johnson term.

Again, integrating noise spectral density from 0.01 hertz through some upper frequency limit to develop the total output noise voltage as a function of bandwidth yields Figure 3.5. Clearly, above 1 kHz total noise is dominated by amplifier voltage noise, and below it is dominated by the photodiode noise. All other noise terms are one and one half to two orders of magnitude lower than the photodiode terms for bandwidth less than 20 hertz.

Figure 3.6 graphs the total output voltage noise for a 76 hertz bandwidth as a function of measured temperature (Eq 2.25). By extrapolation, the SCID signal to noise of 1.0 must be near 200°C compared to the significantly higher value of 340° C for the TIA.

From the above analysis on output voltage noise, it has been established that the amplifier voltage noise is not a limiting factor for these low bandwidth applications. For this reason it is acceptable to ignore it and look at noise currents referred to the input. Figure 3.7 graphs the input signal current along with the related noise currents as a function of measured temperature. These currents have been normalized to a 1.0 hertz bandwidth. The SCID model predicts, from equation 2.25, an order of magnitude improvement over the TIA

at 300°C. Expanding this graph (figure 3.8) for better resolution of the noise terms shows that the photodiode creates a noise floor below 300°C and all other terms are non contributors. Figure 3.9 shows a signal divided by noise of over 10 at 300°C, which is an order of magnitude improvement over the TIA.

Using Eqs 1.0 and 1.3 to convert noise currents into limits of temperature measurement resolution and graphing the results as a function of measured temperature yields Figure 3.10. The SCID model prediction is presented with measured data which demonstrate excellent agreement (Figure 3.10). Figure 3.11 is an expansion of this data at the low temperature end for better clarity. The slight offset at the very low end of the scale is most likely some small extrinsic noise source not completely designed out of the circuit.

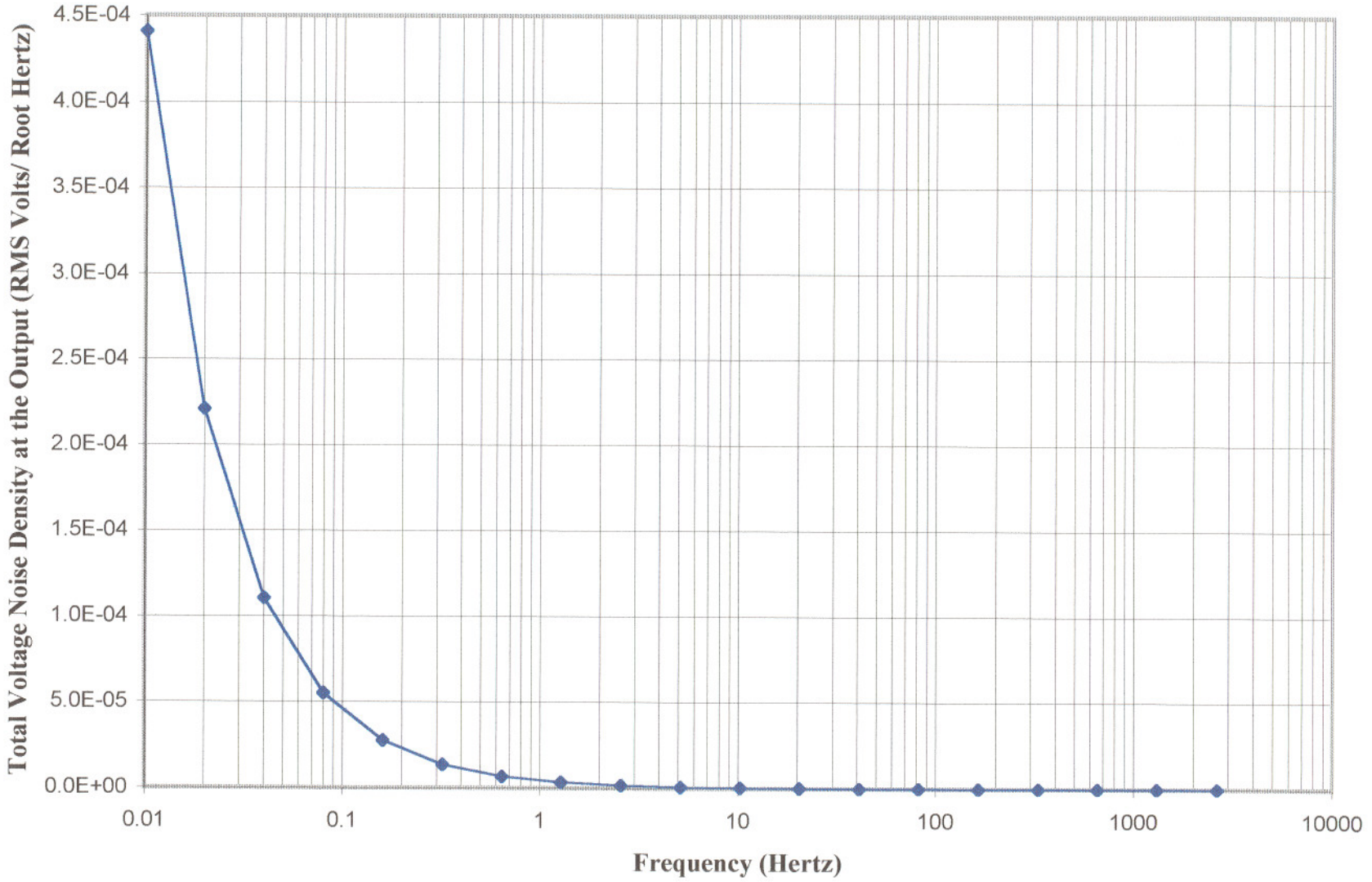

Figure 3.3 Total Noise Voltage Spectral Density Refered to the Output (SCID Model - Equatiion 2.28).

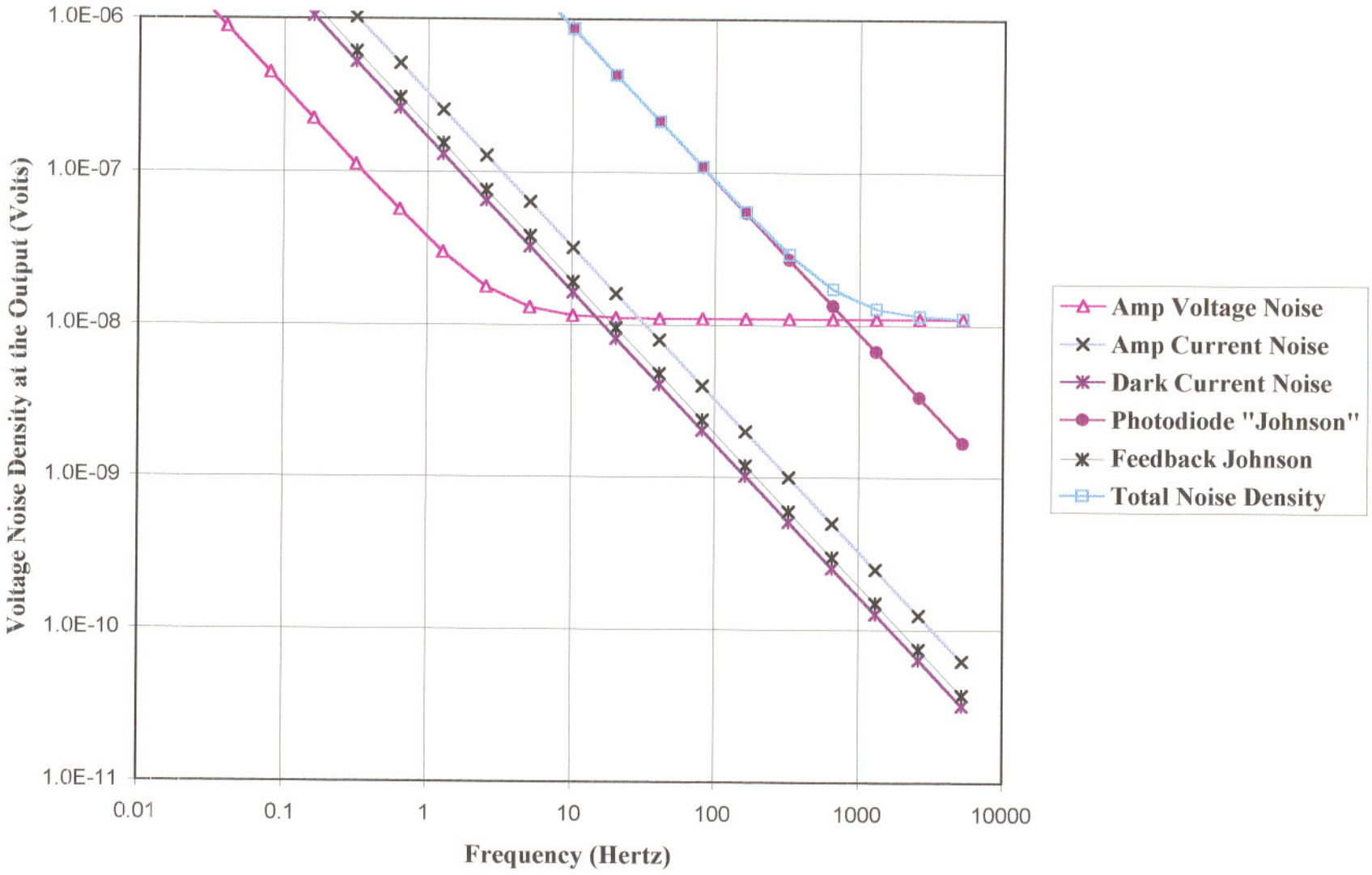

Figure 3.4 Components of Total Noise Voltage Spectral Density for the SCID Model (Equation 2.28).

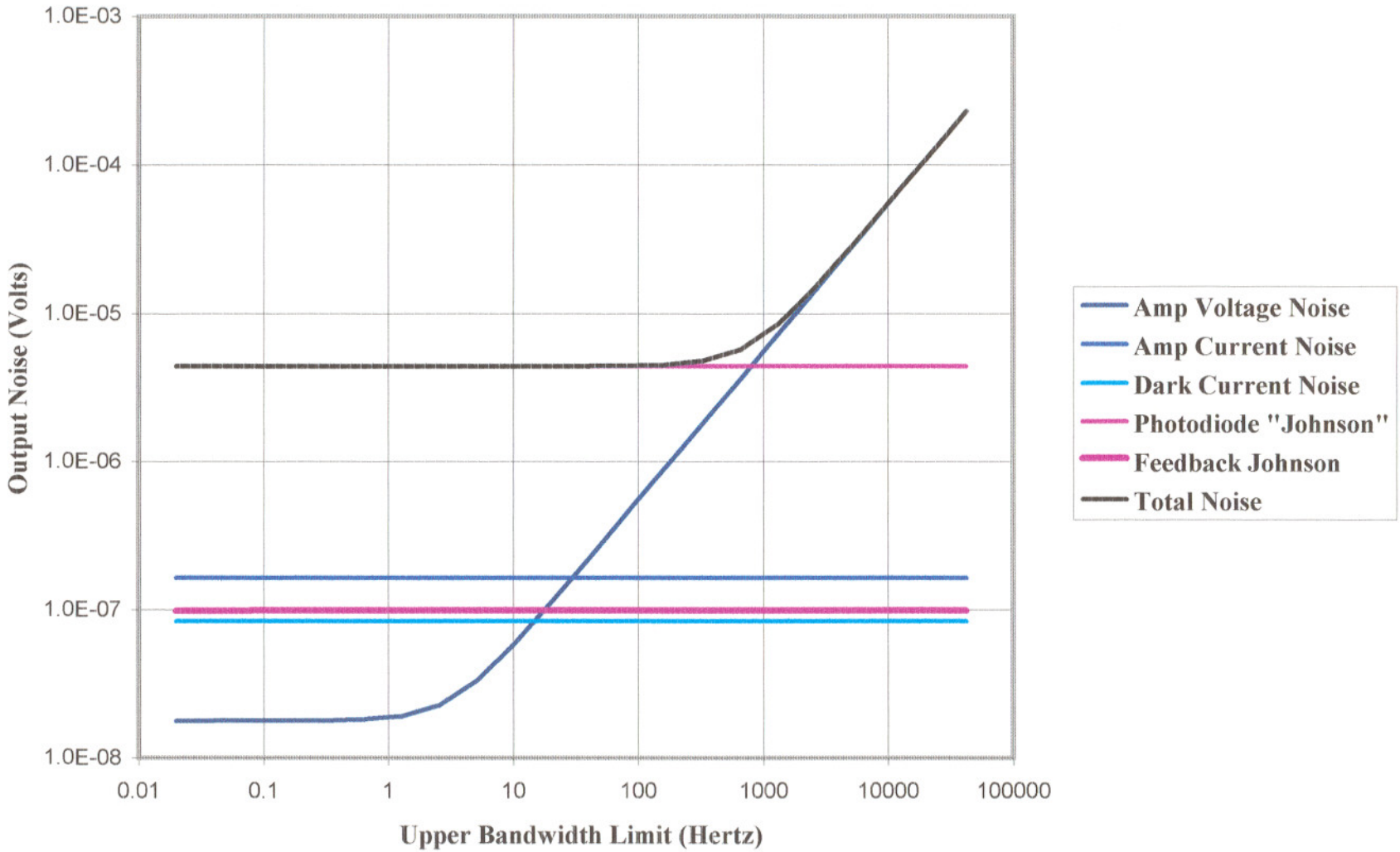

Figure 3.5 Total Output Noise Voltage as a Function of Bandwidth. For the SCID Model with a lower bandwidth limit of 0.01 Hertz.

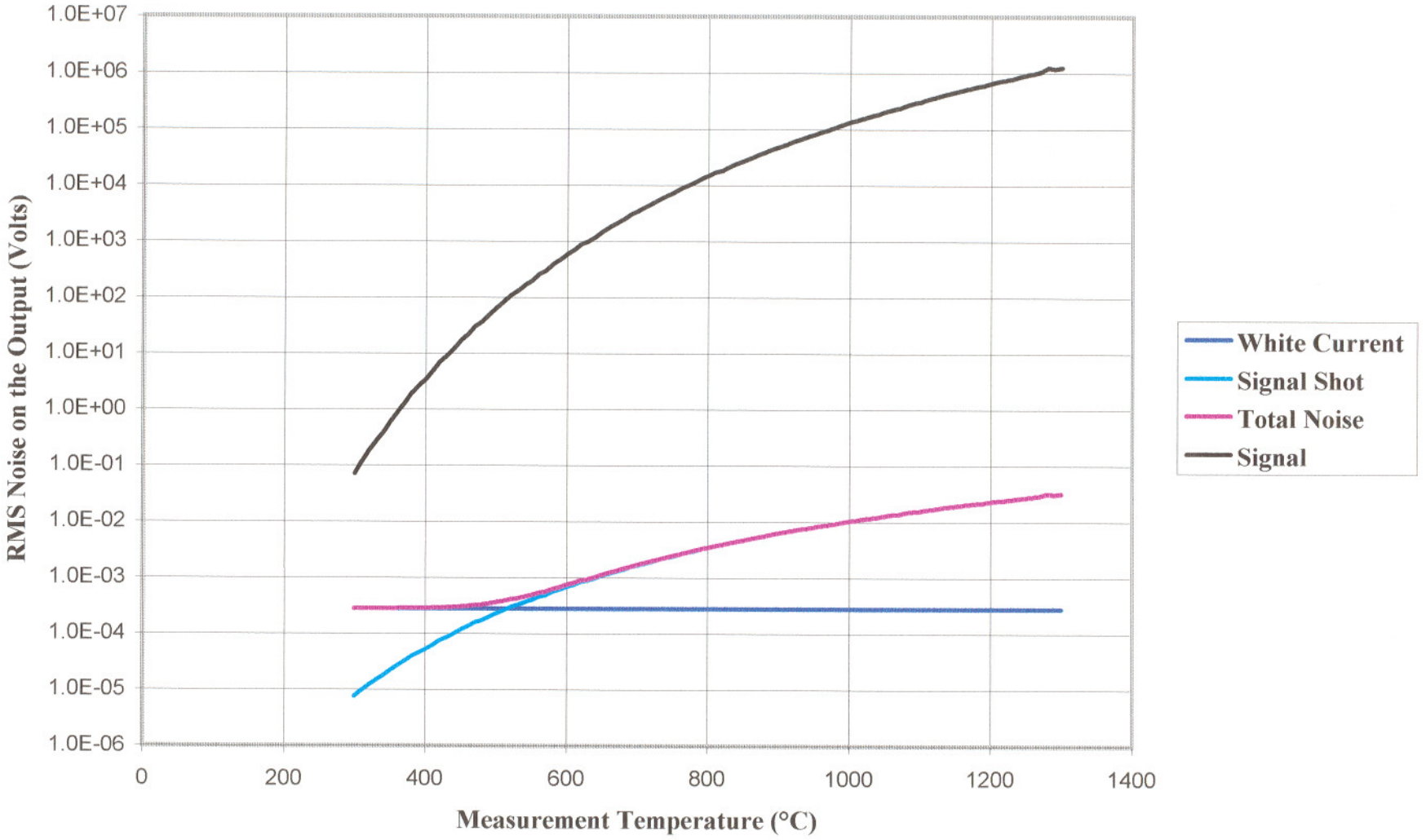

Figure 3.6 Signal and Noise as a Function of Measurement Temperature. For the SCID Model, 76 Hertz Bandwidth, Refered to the Output.

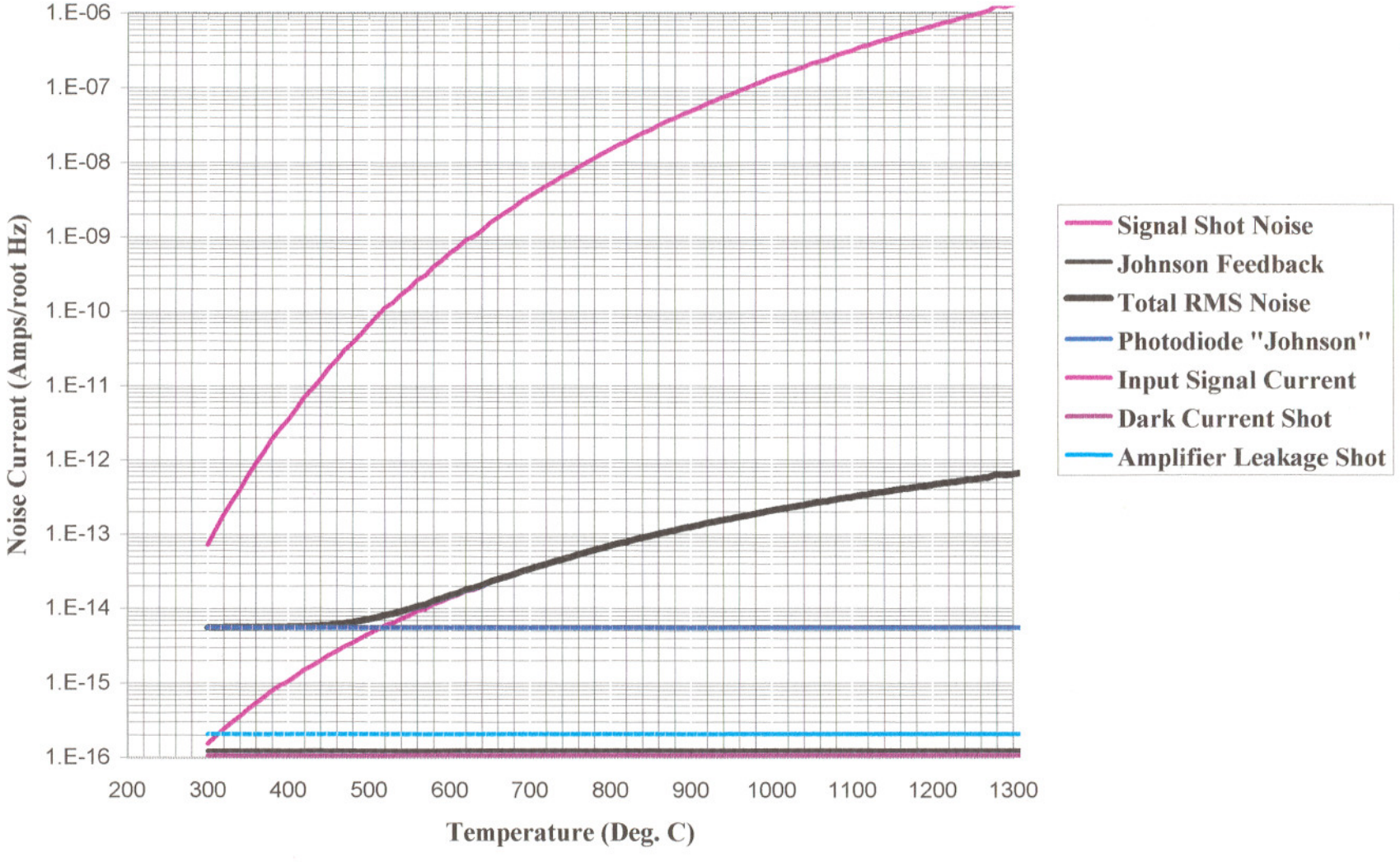

Figure 3.7 Input Signal Current with Related Noise Terms as a Functiion of Measured Temperature (SCID Model, Equation 2.25)

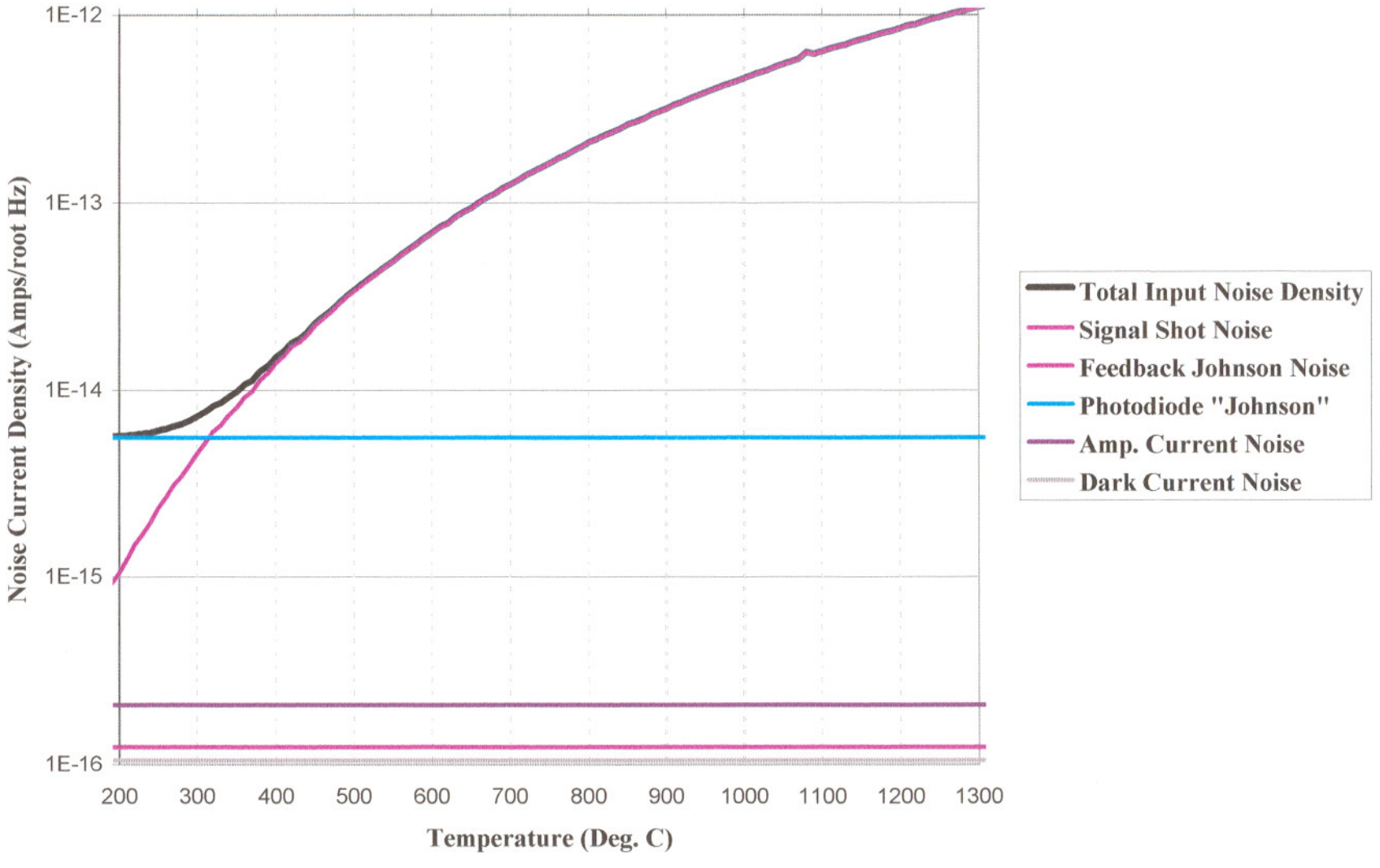

Figure 3.8 Components and Sum of the Input Current Noise Density (SCID Model, Equation 2.25)

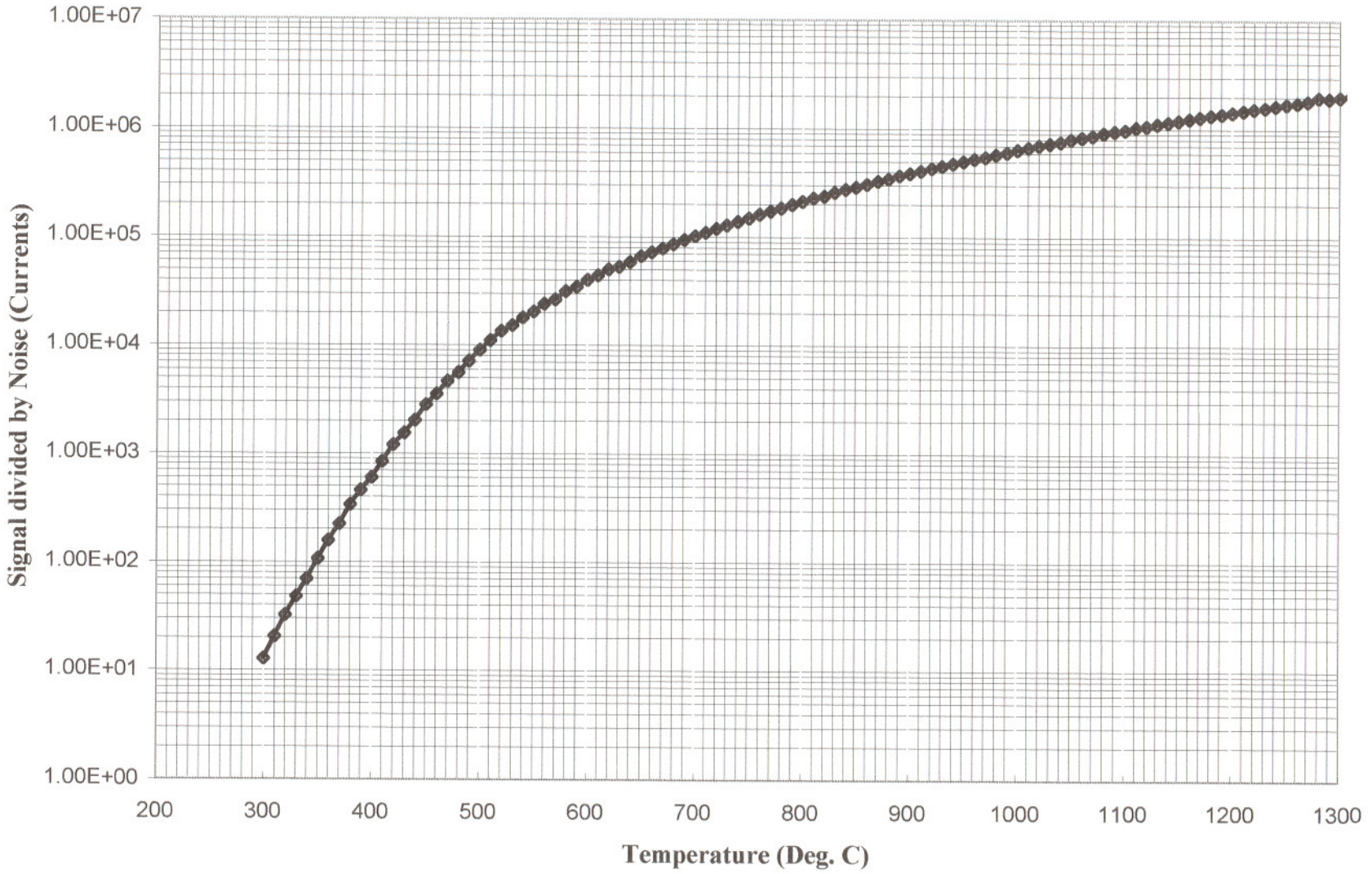

Figure 3.9 Signal Divided by Total Noise (SCID Model, Currents Refered to the Input).

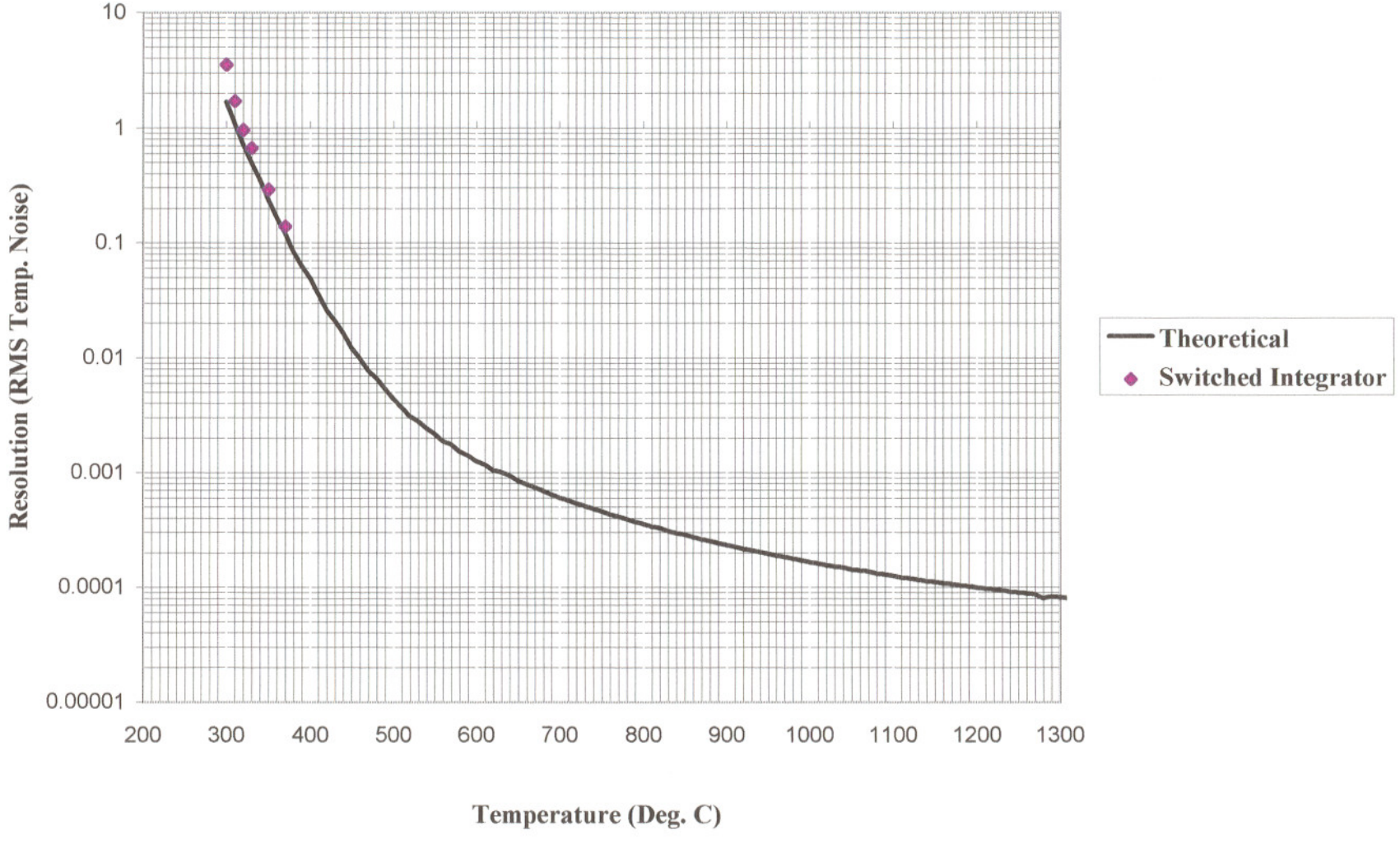

Figure 3.10 Resolution of Temperature as a Function of Temperature Measured (SCID Model, 1 Hertz Sample Rate).

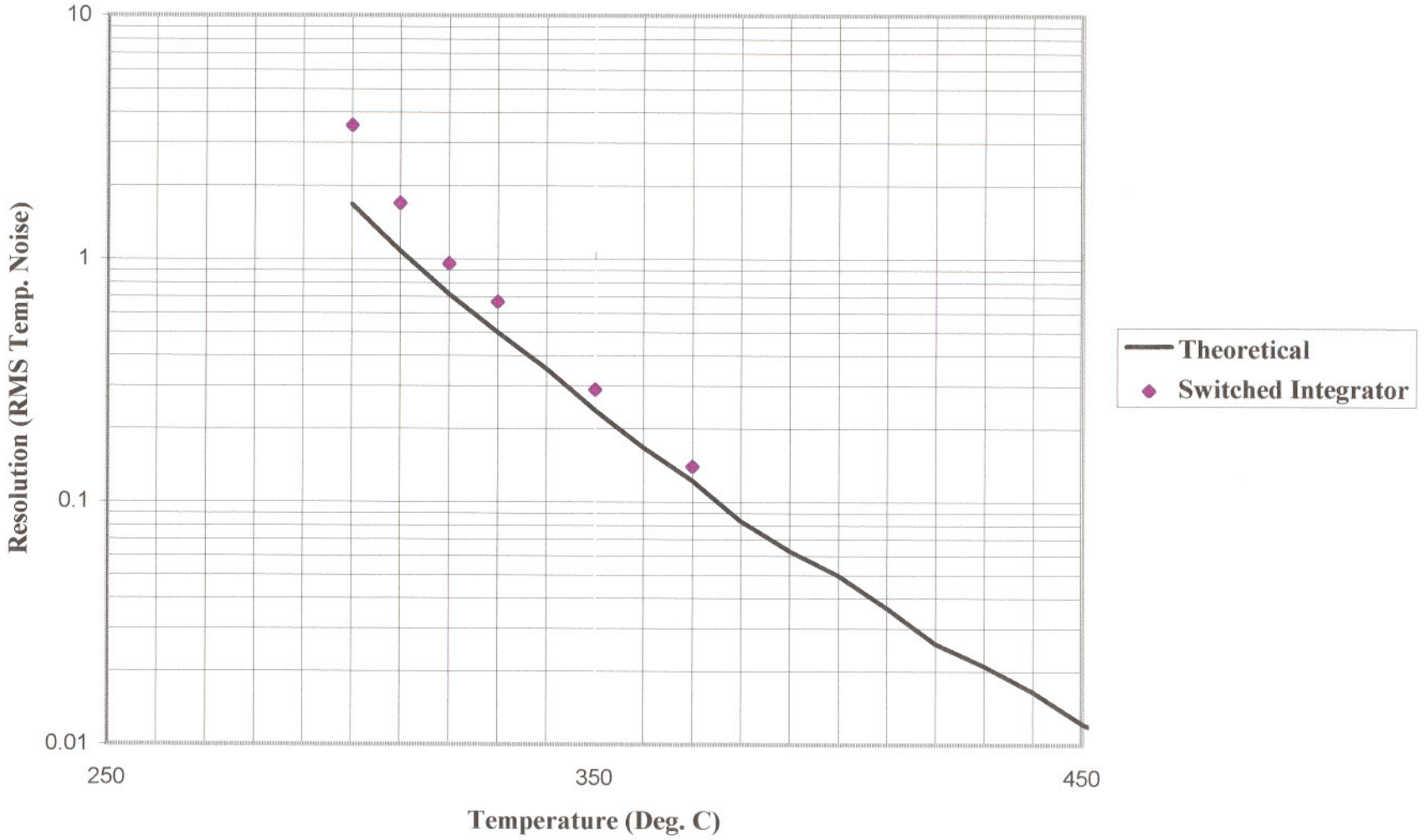

Figure 3.11 Resolution of Temperature as a Function of Temperature Measured (SCID Model, 1 Hertz Sample Rate). Expanded Scale

CHAPTER 4

SUMMARY AND CONCLUSIONS

4.1 The Development of Various SCID Systems.

In the duration of this investigation, four different versions of a SCID system were developed and built. All four systems will be briefly described in the following discussion. The third system was the one used in the mathematical model of Chapter 3 and will be compared to a TIA in the next Section 4.2.

The first SCID was a laboratory setup to demonstrate proof of concept. Cooling was accomplished by submerging the complete optical head assembly and front end electronics in a thermally controlled refrigerated water bath. No constraints of a practical industrial instrument were incorporated into this system. The first quick experiments for feasibility demonstrated the achievement of a 13 kHz bandwidth, and the noise limited resolution at low signal level was better than the existing TIA technology. The experimental design for

the signal/noise study was real simple. A thermal signal was produced by forcing a hot plate to slowly oscillate a few degrees around setpoint. A lightpipe directed toward the hot plate was connected through a 1000μm diameter multimode fiberoptic cable to a silicon photodiode (with no optical filter). The photodiode was connected to the ACF2101 integrator development system and a Nicolet oscilloscope for analog to digital conversion and data storage. The sensor and electronics were shielded electronically, and made water tight by inserting them through a thin latex tube (Penrose surgical drain tube). The output of the ACF2101 was compared to the output from a thermocouple tracking the hot plate to determine the sensitivity of change of mV output per change in degree C. The hotplate control setpoint was lowered in increments of 20°C. When the bath was cooled to near freezing and with hotplate setpoint at 190°C, the peak to peak noise was 0.38°C. Measurements below this temperature were limited by the 12 bit resolution of the Nicolet. This represents about an order of magnitude improvement in the noise current measured at ambient temperatures. Because of throughput differences it is hard to make quantitative comparisons with the M100 TIA, which without an optical filter will resolve about 0.22°C (0.05Hz) at 300°C. This data certainly demonstrated that major improvements in low temperature sensing could be achieved through this technique.

The second system was a simple hybrid design, where both the switched integrating amplifier and the photodiode (both in die form) were mounted upon a two stage (3 watt) thermoelectric cooler. This system consisted of a small hermetically sealed and electrically shielded can. The top housed the optical window and the bottom supported sixteen electrical feedthroughs and a heatsink (see Figure 4.1). As the AFC2101 has two channels on the same die, a second photodetector was incorporated to be used as a reference or as a second channel. Many applications such as Two Color Pyrometry, or Ripple Pyrometry require a second channel. Technical problems in optical crosstalk, and extrinsic noise induced from regulation of the TEC plagued the initial prototypes. Before these issues could be resolved, Burr-Brown stopped selling the ACF2101 in die form, so this design was not pursued further.

The third and forth systems were complete industrial instruments designed for production. They incorporated a very large TEC which cooled the complete optical head and front end electronic assembly. The photodiode and amplifier were used in their standard DIP packages. The third system used a silicon photodetector and had an optical throughput similar to the 1992 version of Accufiber's Model 100, a TIA design. Therefore, the models in this study was developed around this third implementation to allow an "apples to apples" comparison with the well characterized Model 100 TIA.

The forth system used an InGaAs photodetector optimized with higher optical throughput, and more thoughtfully laid out electronics using Burr-Brown's more recent IVC102 switched integrator rather than the ACF2101. This has resulted in a one sigma temperature resolution measurement of 0.26°C at 50°C, 0.48°C at 45°C, and 1.1°C at 40°C. Measurements much below these temperatures will be limited by self emission from the cables, sensors, ferrules, apertures, and reflected ambient background radiation. Previous TIA's with InGaAs detectors obtained similar resolutions at approximately 70°C higher temperatures.

4.2 Comparison of transimpedance and switched integrator technologies.

4.2.1 Bandwidth

For the TIA the bandwidth is determined by the amplifier or more commonly, as in applications considered here, the RC time constant in the feedback loop. For most industrial sensing applications, the electronic noise floor is more limiting than instrument bandwidth, so the RC time constant is adjusted to reduce the noise bandwidth to a minimum referenced to the signal bandwidth.

In the switched integrator, bandwidth is determined by the integration time, as all changes

in signal are averaged within that interval. At the end of integration, the accumulated charge is measured and the capacitor discharged to reset the system for the next measurement. At high sample rates, the measurement and dumping of charge adds a substantial overhead to the cycle time and becomes the dominant factor in limiting the upper bandwidth. Because of the discrete nature of the integrating period the frequency response becomes complex for signal frequencies near or greater than the sample frequency. As the signal frequency increases above the sample frequency, aliasing creates a series of zero response nodes. If there is extrinsic noise at specific frequencies, this can be used to an advantage. For example, if the first node is set to 60Hz then the system will have a zero response to 60Hz and all the upper harmonics of 60Hz. This has been very helpful in limiting power supply and other sources of 60Hz EMI commonly found in industrial settings.

4.2.2 Dynamic Range

In the TIA linear range is limited in the upper end by the power supply voltage and in the lower end generally by the output offset voltage. The range is commonly extended by gain switching, which is accomplished by switching values of feedback resister. Three amplifier stages in cascade can accomplish six orders of magnitude dynamic range by this method of piecewise linear segments. For precision circuits all the gain combinations must be precisely calibrated for gain and offset. As the offset voltage drifts with time, routine automatic recalibration algorithms are sometimes appropriate. Several drawbacks are sometimes encountered with these linear gain switching circuits. With the offset voltage continually drifting, it is hard to assure that all junctions between the segments will be completely seamless. In applications where the signal changes intensity rapidly, gain switching may create dropouts or fail to track the changes altogether. This is the result of the settling time required for the amplifiers to regain stability after a gain change. The precision mercury coated relays occasionally mechanically fail.

In the simplest form of the switched integrator, charge accumulates across the

feedback capacitor for a fixed period of time. The charge is then measured and the capacitor reset for the next integration cycle. Dynamic range can be extended by two methods, changing the integration time or switching the value of the integrating capacitor. The ACF2101 has a 100 picofarad integrating capacitor, with the option of connecting on external values for extending the range. More recent devices have a variety of internal capacitors from which to choose. The amplifiers are laser trimmed to greatly reduce both offset and drift. Charge transfer errors created by switching the capacitor is compensated for (made equal and opposite), and can be reduced to zero by choosing the correct logic sequence of operating modes. The switched integrator can offer nearly seamless operation over a very wide dynamic range within a single electronic stage. At higher input current values, the integration time is short and the reset time become the limiting parameter.

4.2.3 Noise

For the low frequency applications considered here, the only fundamental noise difference between the two technologies is the lack of Johnson noise from the feedback loop in the switched integrator. Great care must be taken in both designs to eliminate extrinsic noise sources, which generally limit circuits designed for general industry. Without the feedback Johnson noise, the switched integrator has the potential of lower noise performance by slight cooling as will be discussed in the following section.

4.3 The Effect of Lowering Temperature on Noise

As can be seen from Figure 3.8 which shows noise current referenced to the input, the photodiode "Johnson" noise determines the noise floor below 200°C, and the signal Shot noise dominates for higher temperature measurements. All noise terms have been substantially lowered by the effects of moderate cooling as summarized in Table 4.1.

Table 4.1 Effects of Modest Cooling on Noise

Noise Source	TIA uncooled	Integrator uncooled	Integrator Cooled to 0°C
Feedback Johnson (amps / root hertz)	4.1E-14	1.3E-16	1.2E-16
Diode "Johnson" (amps / root hertz)	1.4E-14	1.3E-14	1.8E-15
Amp. input current (amps / root hertz)	4.9E-16	1.8E-16	7.5E-17
Amp. input voltage @ output (μV rms)	48	49	0.16
Dark current (amps / root hertz)	2.6E-16	1.3E-15	3.3E-17
Total Input Noise (amps / root hertz)	4.3E-14	1.3E-14	1.8E-15

4.4 Sensitivity to Radiation - Background, Cosmic Rays

It was observed with the SCID that occasionally a large output spike would occur during a single measurement. Various extrinsic noise sources were investigate and eliminated. When the photodiode was replaced with a resistor of the same impedance, the problem vanished. The number of spikes per day (approximately one per hour) was

proportional to the detector area. The effect was greatest with large area silicon detectors and smallest with small area InGaAs detectors.

This behavior is consistent with the photodiode acting as a simple electrometer radiation detector. The sensitivity was calculated in the following way. It has been well worked out that it takes 3.5 eV to produce one electron pair in silicon [58]. An alpha particle with an energy of 5 MeV would produce ($5x10^6$ / 3.5) ion pairs (electrons) per particle or a charge of $2.3x10^{-13}$ coulombs. An alpha particle will give up all its energy within about 5 to 10 micrometers in silicon, which is in the depletion zone of a photodiode in the photovoltaic mode (about 50 micrometers with no bias voltage). This charge is accumulated across the 100 pf integrating capacitor to produce an output voltage of (Q/C) 2.3 millivolts which is just about the observed size of the spikes (Figure 4.1). Most beta particles produced by background radiation will be stopped in about 300 micrometers and produce about 25 thousand electron-hole pairs [59]. Only about 17 percent of the electron will be freed in the depletion region, the rest will likely recombine before they can diffuse to the boundary. Silicon diodes used as particle detectors are reversed biased to extend the depletion region into a large enough volume so that all the energy can be collected. Using the above method of calculation yields only about 6.5 microvolts for a beta particle. Gammas and other sources of ionizing radiation also have very little effect in such a small volume.

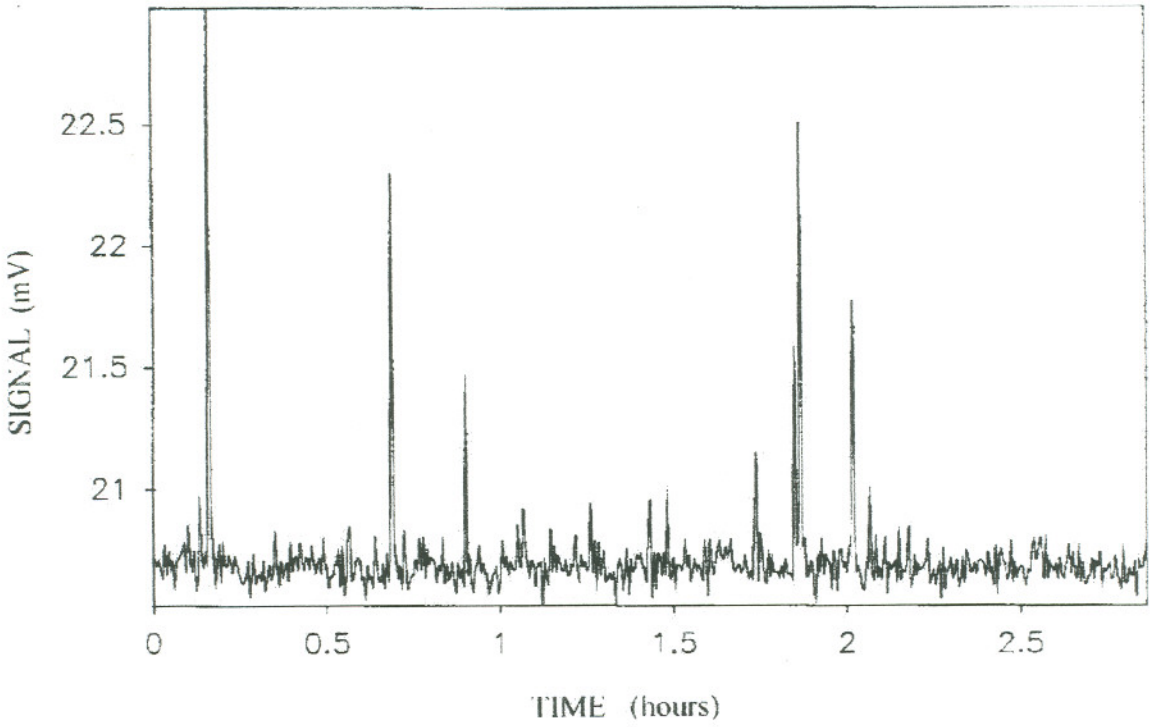

Figure 4.1 Random Noise Spikes in the Feasibility Test Set-Up.

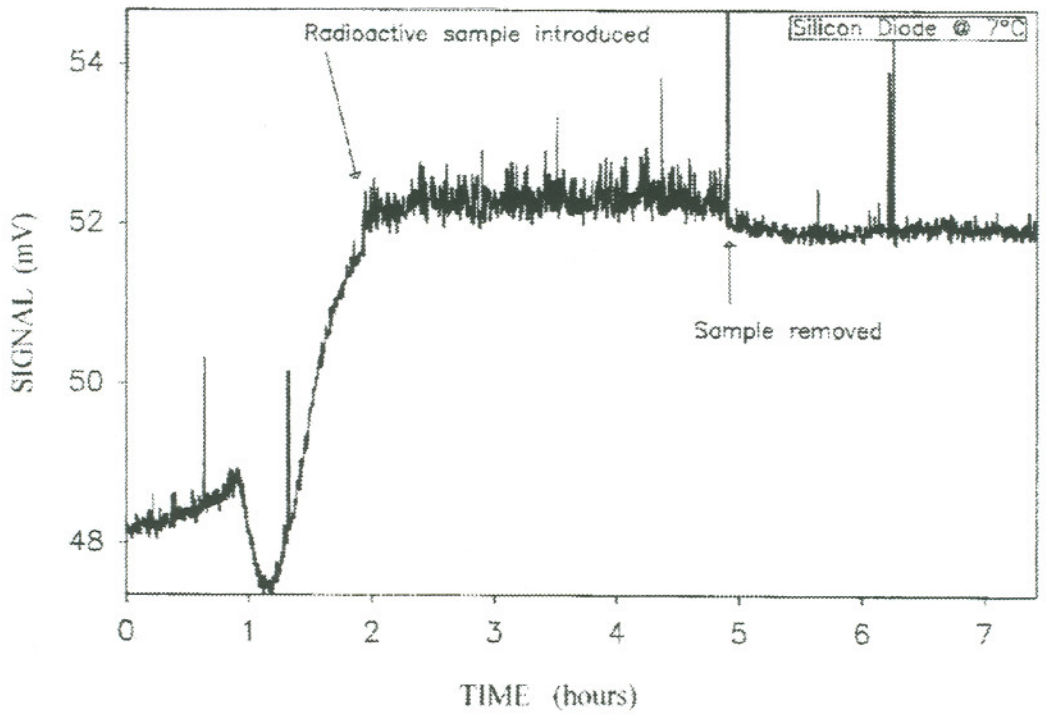

Figure 4.2 Demonstration of Sensitivity to Radioactive Emissions.

To test this theory of radiation sensitivity, a Uranium ore sample was placed in the vicinity of the detector as a qualitative experiment (Figure 4.2). A very distinctive increase in counts (spikes) resulted. It is unlikely that alpha particles from the sample could make it to the detector, but large quantities of beta and gamma rays could. This accounts for the slight shift in baseline and the smaller peak heights observed in this experiment, but demonstrates the sensitivity of this system to ionizing radiation.

It was concluded, although not proven, that the random spikes in the signal were caused by alpha particles from background radiation. A possible source of alpha contamination might be the recirculating water bath, which was purchased from a medical school research facility, where radioactive labels are commonly used. This still does not explain how the contamination reached the detector housing from where alpha particles could reach the detector. For years the semiconductor memory industry was plagued by alpha particles changing the stored charge in a BIT. The problem was ultimately traced to contamination in the packaging material.

There may be some applications where serious errors in measurement and control could result from a single large artifactual reading, and some thoughtful software filter to screen these out may necessary. As an example, systems requiring a rapid control response (Avionics, Aerospace) might limit the effect of a single reading at some threshold amount, rather than as a directly proportional relationship. System in semiconductor processing equipment, where multiple channels are used in the same chamber, may compare channels and exclude any single large outlier.

4.5 Proposing a Hybrid Design

As was mention in section 4.1 a hybrid design was constructed by bounding two photodetectors and a ACF2101 switched integrator in die form directed to the surface of a two stage thermoelectric cooler (see Figure 4.3). This small unit was mounted inside a TO5

can with a quartz input window on top. This design was not completely debugged before Burr-Brown dropped the sale of the AFC2101 in die form. The problems which remained to be solved were the optical cross talk between the two channels, and low frequency drift of the output signal.

The cross talk issue could be completely solved by a thoughtfully designed baffle to contain the light from the fiber onto it respective photodiode. This might be accomplished by the use of a metalized reflective Mylar "tent" which would seal around the edges of the detector and form a dome over it. The fiber optic would penetrate through the top of this film which would redirect any stray light back onto the detector. This film would to too thin to contribute any significant conduction losses to the TE cooler.

Although not rigorously demonstrated, the low frequency drift was probably due to current induced from the control current changes in the TE cooler. After all, the TE cooler is switching amps of current in extremely close proximity to a circuit designed to detect signals in the femtoamp range. The solution may be a very simple one, as the amplifier offset voltage drops from 0.6 volts at ambient to only a few millivolts by 2°C (20 second integration times). At the lower temperature there is therefore almost no sensitivity to temperature change, i.e. the change in offset voltage per change in temperature is small. Small changes in the amplifier temperature around 2°C will not have a major effect on offset voltage because it is already very close to zero. If the TE cooler is run open loop with a fixed current, its second stage output temperature will have a slight dependency on the ambient temperature. As long as the operating temperature remains below 2°C, these changes should have only minor effects on performance. Running the TE cooler with constant current would eliminate any induced current into the SCID circuit.

4.6 Impact on Instrument Design and Performance

The construction of a hybrid design will allow the design and manufacture of a supporting PC board with microprocessor control to manage the logic of the AFC2101 and handle simple I/O functions. This card would form a core technology that could be embedded in a variety of instrumentation from biochemical sensors, spectrometers, radiation monitors, to low temperature short wavelength IR temperature sensors.

There are three major performance improvements which would result from using a SCID. First, it will allow the detection of signals significantly smaller than the traditional transimpedance designs. The second advancement provides continuous processing wide dynamic range transient events, such as combustion, explosions, rotating or fast moving targets. The present instruments use programmable gain amplifiers that cannot track a wide dynamic range of signals during gain switching, as they are limited by the 50ms amplifier settling time that routinly interrupts the amplifier. The third advancement is the increasing of the data acquisition sampling frequency to a minimum of 5 or 10 kHz. The integration time can be adjusted or samples averaged together in software to gain dynamic range. It is possible to develop a system that would yield optimum signal resolution, by continuously trading off bandwidth for resolution in real time as the signal varies in intensity.

4.7 Final Review

This thesis presented the theoretical background to understand the fundamental noise sources in quantum photodetectors and their associated electronics. This understanding was used to analyze, design, construct, and evaluate a practical alternative to the traditional TIA/photovoltaic circuitry. The models developed were verified by good agreement with measured data. SCID designs are currently being developed into practical industrial instruments which will exceed previous performance/cost limits. SCID designs should find

a large variety of applications in low noise signal detection as the concept is developed and matured in the marketplace over time.

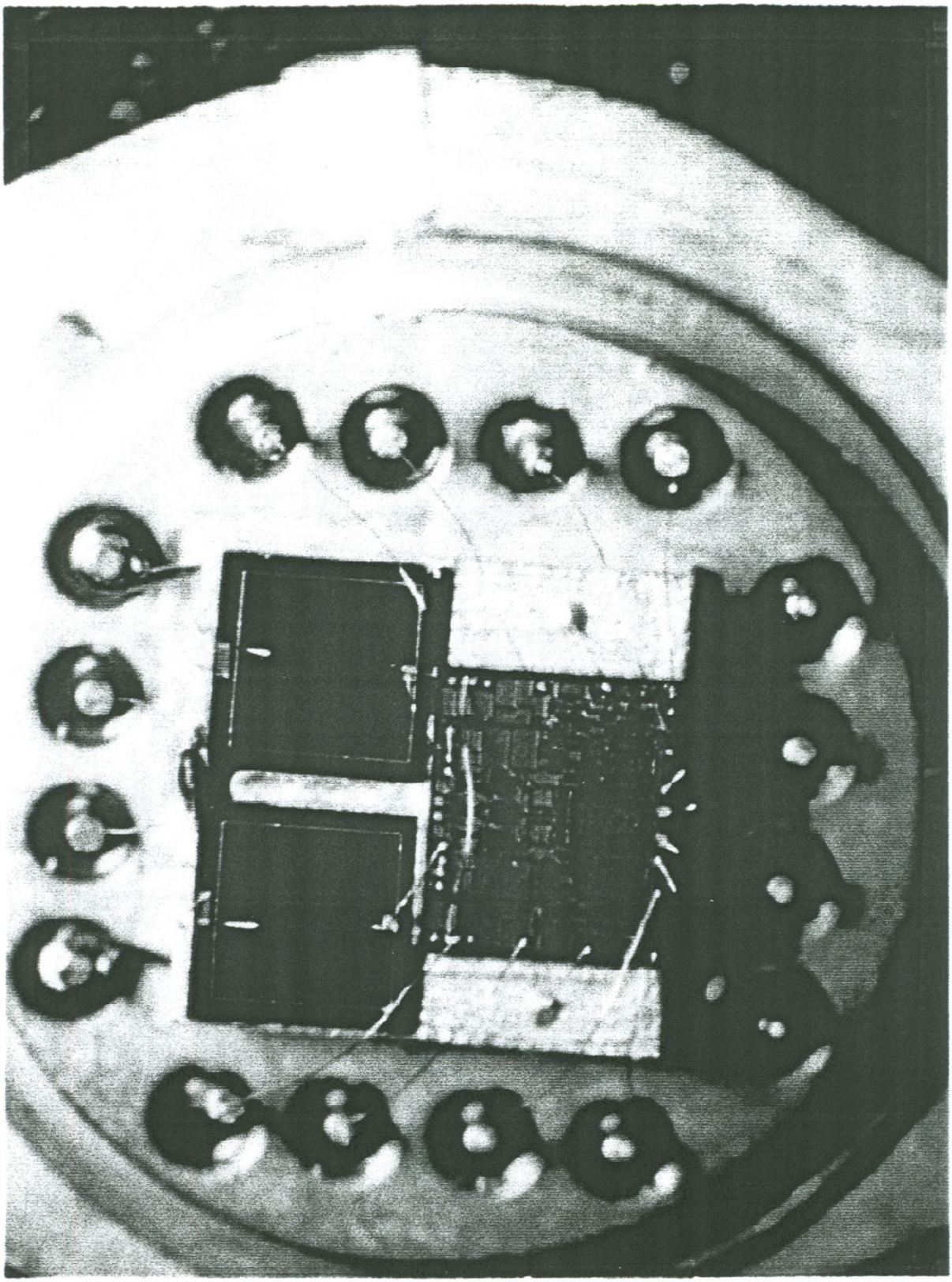

Figure 4.3 Photomicrograph of Thermoelectrically Cooled Hybrid SCID.

Bibliography

1. E.P. Meulenberg, W.H. Mulder, P.G. Stoks, "Immunoassays for Pesticides", *Environmental Science and Technology*, **29** (3), pp553-558, (1995).

2 L.C. Shriver-Lake, R.A. Ogert, F.S. Ligler, "A fiber-optic evanescent-wave immunosensor for large molecules", *Sensors and Actuators B*, **11** (1-3), pp239-243, (1993).

3. P. Oroszlan, G.L. Duveneck, M. Ehrat, H.M. Widmer, "Fiber-optic Atrazine immunosensor", *Sensors and Actuators B*, **11** (1-3), pp301-305, (1993).

4. F.G. Tinsley, B.E. Adams, "Evolution in the Application of Optical Fiber Thermometry (OFT).", *Instrument Society of America , Publication 91-0307*, pp85-111, (1991).

5. B.E. Adams, "Optical Fiber Thermometry for use at High Temperatures.", *Temperature. Its Measurement and Control in Science and Industry Vol 6, pt 2*, American Institute of Physics, pp 739-743, (1992).

6. E. Ishikawa, "Ultrasensitive Enzyme Immunoassay", *Immunochemical Assays and Biosensor Technology for the 1990s*, R. M. Nakamura, Y. Kasahara, G. A. Rechnitz Edts., pp183 - 203, American Society for Microbiology, Washington, DC, (1992).

7. R.P. Richards, D.B. Baker, "Atrazine Exposure through Drinking Water: Exposure Assessment for Ohio, Illinois, and Iowa.", *Environmental Science and Technology*, **29** (2), pp406-412, (1995).

8. P. Oroszlan, G.L. Duveneck, M. Ehrat,H.M. Widmer, "Automated Optical Sensing System for Biochemical Assays.", *SPIE Proceedings*, Vol 2068, pp159-168, (1994).

9. P.J. Timans, "The thermal radiative properties of semiconductors" Chapter 2, *Advances in Rapid Thermal and Integrated Processing*, Fred Roozenboom editor, Kluwer Academic Publishers, The Netherlands, (1996).

10. C. Schietinger, B.E Adams, C. Yarling, "Ripple Technique: A Novel Non-Contact Wafer Emissivity and Temperature Measurement Method for RTP". *Rapid Thermal and Integrated Processing.*, Mat. Res. Soc. Symp. Proc., **224**, pp23-31, (1991).

11. Z. Wang, C. Schietinger, B.E .Adams, "Emittance Compensated RTP Temperature Measurement Principles and Practice.", *Proceedings of the Intl. Conf. on Advanced Thermal Processing of Semiconductors - RTP'93*, pp 93-98, (1993).

12. A.T. Fiory, C. Schietinger, B.E. Adams, F.G. Tinsley, "Optical Fiber Pyrometry with In-Situ Detection of Wafer Radiance - Accufiber's Ripple Method.", *Mat. Res. Soc. Symp. Proc.*, **303**, pp139-145, (1993).

13. C. Schietinger, B.E. Adams, "A Review of Wafer Temperature Measurement Using Optical Fibers and Ripple Pyrometry", *Proceedings of the 5th Intl. Conf. on Advanced Thermal Processing of Semiconductors - RTP'97*, New Orleans, pp335-339, (1997).

14. T. Sato, "Spectral emissivity of silicon", *Japanese Journal of Applied Physics*, **6** (3), pp339-347 (1967).

15. W. Schottky, "Űber spontsne Stromschwankungen in verschiedenen Elektrizitäcsleitern (On Spontaneous Current Fluctuations in Different Conductors)", *Annalen der Physik*, Germany, **57**, pp541-567, (1918).

16. C. Delaney, *Electronics for the Physicist*, Penguin Books Inc., pp238-251, (1969).

17. H. W. Ott, *Noise Reduction Techniques in Electronic Systems*, John Wiley & Sons, pp198-213 and pp236-244, (1975).

18. D.A. Bell, *Noise and the Solid State*, John Wiley and Sons, Chapters 1-2, (1985).

19. R.A. Smith, F.E. Jones, R.P. Chasmar, *The Detection and Measurement of Infrared Radiation*, Oxford at the Clarendon Press, Chapter 5, (1957).

20. A. Van der Ziel, *NOISE*, Prentice-Hall Inc., pp 1-7, (1954).

21. P. Horowitz, W. Hill, *The Art of Electronics*, Cambridge University Press, pp 431-438, (1989).

22. J.D. Vincent, *Fundamentals of Infrared Detector Operation and Testing*, John Wiley & Sons, pp 59-62, (1990).

23. C.D. Motchenbacher, J.A. Connelly, *Low-Noise Electronic System Design*, John Wiley & Sons Inc., pp17-37, (1993).

24. P.N.J. Dennis, *Photodetectors: An Introduction to Current Technology*, Plenum Press, pp14-24, (1986).

25. H. Nyquist, "Thermal Agitation of Electronic Charge in Conductors", *Physical Review*, **32** (110), p110, (1928).

26. J. Kertesz and L.B. Kiss, "Noise spectrum in the model of self-organized criticality", *Journal of Physics A*, **23** (9), letters pp L433-L440, (1990).

27. E.W. Montroll, M.F. Shlesinger, "Maximum entropy formalism, fractals, scaling phenomena, and 1/f noise: a tale of tails", *Journal of Statistical Physics*, **32** (2), pp209-230, (1983).

28. K.P. O'Brien, M.B. Weissman, "Statistical signatures of self-organization", *Physical Review A*, **46** (8), pp4475-4478, (1992).

29. S.B. Lowen, M.C. Teich, "Fractal shot noise", *Physical Review Letters*, **63** (17), pp1755-1759, (1989) .

30. B.J. West, M.F. Shlesinger, "On the ubiquity of 1/f noise" , *International Journal of Modern Physics B*, **3** (6), pp795-819, (1989).

31. E. Milotti, "Linear processes that produce 1/f or flicker noise", *Physical Review E*, **51** (4), pp3087-3092, (1995).

32. H. J. Jensen, "1/f noise from the linear diffusion equation", *Physica Scripta*, **43** (6), pp593-595, (1991).

33. R. Voss, "Evolution of Long-Range Fractal Correlations and 1/f Noise in DNA Base Sequences", *Physical Review Letters*, **68** (25), pp3805--3808, (1992).

34. M. Usher, M. Stemmler, Z. Olami, "Dynamic Pattern Formation Leads to 1/f noise in Neural Populations", *Physical Review Letters*, **74** (2), pp326-329, (1995).

35. C.K. Peng, J. Mietus, J.M. Hausdorff, S. Havlin, H.E. Stanley, A.L. Goldberger, "Long-Range Anticorrelations and Non-Gaussian Behavior of the Heartbeat", *Physical Review Letters*, **70** (9), 1343-1346, (1993).

36. T. Belloni, G. Hasinger, "Variability in the Noise Properties of Cygnus X-1.", *Astronomical Astrophysics*, **227** (2), ppL33-L36, (1990).

37. W.H. Matthaeus, M.L. Goldstein, Low-frequency 1/f noise in the interplanetary magnetic field, *Physical Review Letters*, **57** (4), pp495-498, (1986).

37. W.H. Matthaeus, M.L. Goldstein, Low-frequency 1/f noise in the interplanetary magnetic field, *Physical Review Letters*, **57** (4), pp495-498, (1986).

38. R.F. Voss and J. Clarke, "1/f noise in music: music from 1/f noise", *Journal of Acoustical Society of America*, **63** (1), pp258-263, (1978).

39. M.Y. Choi, H.Y. Lee, "Traffic flow and 1/f fluctuations", *Physical Review E*, **52** (6), pp5979-5984, (1995).

40. Xingzhi Zhang, Gang Hu, "1/f noise in a two-lane highway traffic model", *Physical Review E*, **52** (5), pp4664-4668, (1995).

41. T. Musha, H. Higuchi, "The 1/f fluctuation of a traffic current on an expressway", *Japanese Journal of Applied Physics*, **15** (7), pp1271-1275, (1976).

42. G. Peng, H.J. Herrman, "Density waves and 1/f density fluctuations in granular flow" *Physical Review E*, **51** (3), pp1745-1756, (1995).

43. K. Hkadky, J.L. Dawson, *The Measurement of Corrosion using Electrochemical 1/f Noise*. Corrosion and Protection Centre, University of Manchester Institute of Science and Technology, Sackville Street, Manchester M60 1QD, U.K. (1997)

44. J.M. Halley, "Ecology, Evolution and 1/f Noise", *Tree*, **11** (1), pp33-37 (January 1996).

45. S. L. Pimm and A. Redfearn, "The variability of population densities", *Nature*, **334** (18), pp613-614, (August 1988).

46. M. A. Azhar, K. Gopala, "1/f Fluctuations in Beta- Decay of 90Y", *Physical Review A*, **44** (2), pp1044-1048, (1991).

47. T. Musha, "Power Spectral Density Estimation of Light Intensity Fluctuations in Photon Counting", *Japanese Journal of Applied Physics*, **26** (12), pp2022-2025, (1987).

48. J.Y. Campbell, A.W. Lo, A.C. MacKinlay, *The Econometrics of Financial Markets*, Princeton University Press. pp 1-35, (1997)

49. N. Rosario, H. Mantegna, E. Stanley, "Turbulence and financial markets" , *Nature*, **383** (17), pp587-588, (1996).

50. EG&G, Silicon Photodiode [Catalog], *Application Notes*, (1998).

51. Intusoft, *IsSPICE4, ICAP 4 Model Library Listings*, San Pedro, Ca (1994).

52. Burr-Brown Corp., Product Data Sheet for OPA111, Document # 10526, (1993).

53 Hamamatsu Corp., Data Sheet for S1337-66Q photodiode, (1992).

54. B.C. Barker, , "Comparison of Noise Performance between a FET Transimpedance Amplifier and a Switched Integrator.", *Burr-Brown Application Bulletin* AB-057A, (1992).

55. EG&G Optoelectronics, Wellesley, Ma., *Silicon Photodiode Application Notes*, c. 1997, (http://www.egginc.com/bin/webmate/Opto|106/page/egg/sidapp), viewed Aug. 26, 1998.

56. "Accufiber Optical Fiber Thermometer Temperature Resolution.", *Accufiber Application Note* AN-04, Santa Clara, CA., (1988).

57. C. Scheitinger, Luxtron Corp., Portland, Or., Personal Communication, (1998).

58. G.L. Miller, Lucent Technologies, Murray Hill, N.J., Personal Communication , (1998).

59. D. Dorfan, Santa Cruz Institute of Particle Physics, UCSC, Personal Communication, (1998).

Biography

Mr. Adams was born April 22, 1945 in Portland Oregon. He graduated with honors from Benson Polytechnic High School with a major in electronics and from Wheaton College (Wheaton, Illinois) with a BA in Physics. In 1967 he was a member of the United States Antarctic Research Team collecting data to substantiate the continental drift theory. Much of his career has been in medical research or the design of medical instrumentation. These medical design areas include: x-ray image intensifiers, pulmonary function equipment for children, and fiber optic immunosensors. Areas of medical study include: Pulmonary gas diffusion, Alpha 1 - Antitrypsin Deficiency, and POMC peptides. Mr. Adams has taught Astronomy at Concordia College, and Electronics for Technicians at OHSU. He spent about ten years improving fiber optic temperature measurement, including co-inventing of the Ripple Pyrometer. Currently, he is a member of the technical staff for Applied Materials, concerned with the measurement and calibration of temperature during semiconductor processing. His interest have ranged from hang gliding, beekeeping, snowcamping, Soap Box Derby racing, and children's science education.

Invited Seminars and Talks

1. Swedish Temperature Measurement Seminar; Sweden, (1993).
2. Sandia National Laboratories, Albequeque, (1996).
3. ASTM, San Diego, (1997).

Patents

5.769,540	Non-Contact Optical Techniques for Measuring Surface Conditions (June 23, 1998).
5,490,728	Non-Contact Techniques For Temperature Measurement. (Feb. 13, 1996).
5,364,186	Thermally fused composite ceramic blackbody temperature probe and method therefor (Nov. 15, 1994).
5,318,362	Non-contact techniques for measuring temperature for radiation-heated objects (June 7, 1994).
5,310,260	Non-contact optical techniques for measuring surface conditions (May 10, 1994).
5,183,338	Temperature measurement with combined photo-luminescent and blackbody sensing techniques (Feb. 2, 1993).
5,166,080	Techniques for measuring the thickness of a film formed on a substrate (Nov. 24, 1992) .
5,154,512	Non-contact Techniques for measuring temperature on radiation heated objects (Oct. 13, 1992).
5,112,137	Temperature measurement with combined photo-luminescent and blackbody sensing techniques (May 12, 1992).

Publications

C. Schietinger, B.E. Adams, "A Review of Wafer Temperature Measurement Using Optical Fibers and Ripple Pyrometry", *Proceedings of the 5th Intl. Conf. on Advanced Thermal Processing of Semiconductors - RTP'97*, New Orleans, pp 335-339, (1997).

Z. Wang, C. Schietinger, B.E .Adams, "Emittance Compensated RTP Temperature Measurement Principles and Practice.", *Proceedings of the Intl. Conf. on Advanced Thermal Processing of Semiconductors - RTP'93*, (1993).

Z.. Wang, B.E. Adams, F.G.Tinsley, "Transfer Theory for Instrument Applications of Large Core Optical Fiber". *SPIE, Intl Symp on Optics, Imaging, and Instrumentation.*, (July 1993) .

A.T. Fiory, C. Schietinger, B.E. Adams, F.G. Tinsley, "Optical Fiber Pyrometry with In-Situ Detection of Wafer Radiance - Accufiber's Ripple Method.", *Mat. Res. Soc. Symp. Proc.*, **303**, pp 139-145, (1993).

B.E. Adams, "Optical Fiber Thermometry for use at High Temperatures.", *Temperature. Its Measurement and Control in Science and Industry Vol 6, pt 2*, American Institute of Physics, pp 739-743, (1992).

F.G. Tinsley, B.E. Adams, "Evolution in the Application of Optical Fiber Thermometry (OFT).", *Instrument Society of America* , publication 91-0307, pp85-111, (1991).

C. Schietinger, B.E Adams, C. Yarling, "Ripple Technique: A Novel Non-Contact Wafer Emissivity and Temperature Measurement Method for RTP". *Rapid Thermal and Integrated Processing., Mat. Res. Soc. Symp. Proc.*, **224**, (1991).

C.Schietinger, B.E.Adams, "Reliability Improvement Methods for Sapphire Fiber Temperature Sensors.", *SPIE*, Vol. 1366, pp284-93, (1990).

A.S. Buist, B.E. Adams, A.H. Azzam, G.J. Sexton, "Pulmonary Function in Young Children with Alpha 1 - Antitrypsin Deficiency.", *Am Rev Respir Dis*, **122**, pp817-822, (1980).

A.S.Buist, B.E.Adams, A.H.Azzam, and G.J.Sexton., "Reference Values for Functional Residual Capacity and Maximal Expiratory Flow in Young Children.", *Am Rev Respir Dis*, **122**, pp983-988, (1980).

A.S.Buist, B.E.Adams, A.H.Azzam, and G.J.Sexton, "Pulmonary Function in Heterozygotes for Alpha 1 - Antitrypsin Deficiency: A Case-Control Study.", *Am Rev Respir Dis*, **120**, pp759-766, (1979).

B.E.Adams, "Optimizing Single Crystal Aluminum Growth as a Function of Stress.", Senior Research Thesis, Wheaton College, Wheaton Illinois, (1966).